

AD-A146 550

ANISOTROPY AND RELAXATION EFFECTS OF CO₂⁺ IONS IN LITI
FERRITE(U) MASSACHUSETTS INST OF TECH LEXINGTON LINCOLN
LAB G F DIONNE 15 AUG 84 TR-688 ESD-TR-84-034

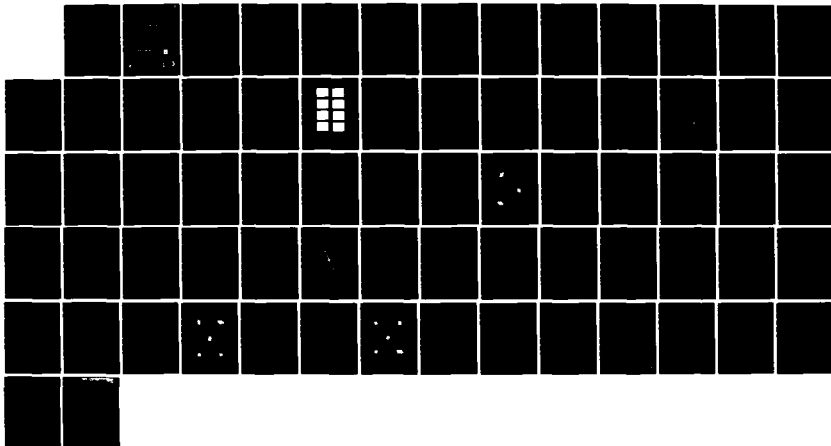
1/1

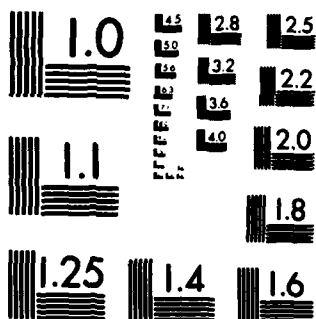
UNCLASSIFIED

F19628-80-C-0002

F/G 20/3

NL





OPY RESOLUTION TEST CHART

AD-A146 550

DTIC
SELECTE
DTIC 16

S

D

E

11 004

The work reported in this document was performed at Lincoln Laboratory, a center for research operated by Massachusetts Institute of Technology. This program is sponsored by the Ballistic Missile Defense Sentry Project Office, Department of the Army, under Air Force contract F19628-80-C-0002.

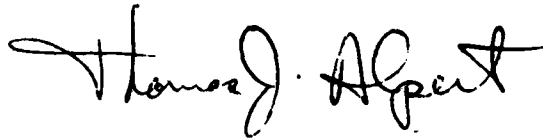
This report may be reproduced to satisfy needs of U.S. Government agencies.

The views and conclusions contained in this document are those of the contractor and should not be interpreted as necessarily representing the official policies, either expressed or implied, of the United States Government.

The Public Affairs Office has reviewed this report, and it is releasable to the National Technical Information Service, where it will be available to the general public, including foreign nationals.

This technical report has been reviewed and is approved for publication.

FOR THE COMMANDER

A handwritten signature in black ink, reading "Thomas J. Alpert". The signature is fluid and cursive, with the first name "Thomas" and last name "Alpert" clearly legible.

Thomas J. Alpert, Major, USAF
Chief, ESD Lincoln Laboratory Project Office

Non-Lincoln Recipients
PLEASE DO NOT RETURN

Permission is given to destroy this document
when it is no longer needed.

MASSACHUSETTS INSTITUTE OF TECHNOLOGY
LINCOLN LABORATORY

ANISOTROPY AND RELAXATION EFFECTS
OF Co^{2+} IONS IN LiTi FERRITE

G.F. DIONNE

Group 33



TECHNICAL REPORT 688

15 AUGUST 1984

Accession For	
NTIS GRA&I	<input checked="" type="checkbox"/>
DTIC TAB	<input type="checkbox"/>
Unannounced	<input type="checkbox"/>
Justification	
By _____	
Distribution/	
Availability Codes	
Special and/or	
Dist	Special
A-1	

Approved for public release; distribution unlimited.

LEXINGTON

MASSACHUSETTS

ABSTRACT

— Microwave power absorption and hysteresis loops were studied on a series of ferrite materials prepared from a standard LiTi spinel host with $\text{Co}^{(2+)}_{\text{I}}$ additions in amounts up to 0.05 ions per formula unit. Experimental results over this concentration range indicate that the rapid relaxation of $\text{Co}^{(2+)}_{\text{I}}$ causes X-band peak power thresholds to increase by a factor of more than 100 and magnetic loss parameters by a factor greater than ten. The usual strong effects of $\text{Co}^{(2+)}_{\text{I}}$ positive magnetic anisotropy, however, were not found in either ferrimagnetic resonance linewidths or hysteresis loop parameters. As a consequence, it is concluded that peak power thresholds can be raised substantially by $\text{Co}^{(2+)}_{\text{I}}$ additions with a modest penalty in magnetic loss, but without the catastrophic deterioration of the hysteresis loop observed previously in undiluted lithium ferrite.

To account for the absence of anisotropy effects in the presence of strong relaxation effects, Co^{2+} is considered to act as a paramagnetic ion through decoupling from the exchange fields of the iron sublattices. This new theory of exchange isolation is based on selective clustering of dilutant ions that results from minimization of magnetic exchange, lattice electrostatic, and crystal field stabilization energies. The model is tested by comparing its predictions with the published results of a variety

of experiments on both the lithium-titanium spinel and the calcium-vanadium garnet systems.

TABLE OF CONTENTS

Abstract	iii
I. INTRODUCTION	1
II. EXPERIMENTAL PROCEDURE	3
A. Sample Preparation	3
B. Measurements	5
III. EXPERIMENTAL RESULTS	6
IV. EXCHANGE ISOLATION OF Co^{2+}	9
V. CATION CLUSTERING MECHANISMS	19
A. Magnetic Exchange Energy	22
B. Lattice Electrostatic Energy	23
C. Crystal Field Stabilization Energy	27
VI. DISCUSSION AND CONCLUSIONS	31
A. Anisotropy and Hysteresis Loops	32
B. Relaxation Effects	36
C. Cobalt Effects in Garnets	37
APPENDIX A - Dependence of Anisotropy on Co^{2+} Exchange Coupling	45
APPENDIX B - Oxygen Parameter Calculations	49
APPENDIX C - d-Orbital Wave Functions in Axial Crystal Fields	51
APPENDIX D - Effects of Zn^{2+} on Magnetization and Anisotropy Fields of LiTi Ferrite	57
Acknowledgments	61
References	63

I. INTRODUCTION

The divalent cobalt ion (Co^{2+}) in ferrimagnetic oxides has been a subject of investigation for at least three decades. Since this ion exhibits unusually large magnetoelastic coupling in octahedral sites, it has been substituted into ferrimagnetic oxides where its strong contribution to magnetic anisotropy, magnetostriction, and ferrimagnetic relaxation could be studied. These effects have proven to be important for computer memories, recording materials, and microwave devices and absorbing materials. As a consequence, the results of much research have been reported over the years for a variety of host lattices.

Cobalt anisotropy effects in the nickel spinel ferrite family have been investigated by Bozorth et al. [1] and in the $\text{Co}_x\text{Fe}_{3-x}\text{O}_4$ (magnetite) system by Bickford et al [2]. However, it is principally in the lithium ferrite family [3,4] and to a lesser extent in the garnet lattice [5-8] that most of the recent interest has been focused. Based on the results of microwave high power measurements, Co^{2+} ions in ferrite compositions are believed to be responsible for raising dramatically the spinwave instability threshold because of their rapid spin-lattice relaxation properties [3,9-12]. This phenomenon is extremely useful in designing materials for high power microwave devices. In at least one case, however, this benefit does not come without a

price. According to Van Hook and Dionne [13], the hysteresis loop of $\text{Fe}[\text{Li}_{0.5-x/2}\text{Co}_x\text{Fe}_{1.5-x/2}]_4\text{O}_4$ degrades sharply at room temperature for values of $x \geq 0.015$. Since this threshold concentration of Co^{2+} represents the amount required to cancel the negative anisotropy of lithium ferrite [14], the explanation of these catastrophic effects on the hysteresis loop was based on the role of anisotropy in creating reverse domains at or near the remanent state. These results suggested that the concentrations of Co^{2+} in lithium ferrite would have a practical upper limit determined by x_c , the concentration value for anisotropy cancellation.

In an earlier study, however, Banerjee et al. [15] had found that anisotropy cancelling Co^{2+} concentrations determined from ferrimagnetic resonance linewidth measurements of magnetically diluted lithium ferrite produced conflicting results. For pure lithium ferrite, $x_c = 0.015$, in accord with the accepted value. For an aluminum-substituted composition, x_c fell not surprisingly to 0.007, but for a titanium-substitution there was no detectable anisotropy cancellation up to $x = 0.02$. These effects were also seen in the recent work by Brower and Patton [4]. The interpretation of this unexpected phenomenon will be analyzed in a new model to be introduced in a later section, but for the moment it is sufficient to assume that Ti^{4+} ions serve to disrupt the normally strong positive anisotropy contributions from Co^{2+} in these

materials. With this possibility as a premise, we must consider whether the hysteresis loop characteristics of lithium-titanium ferrite will also be immune from the dramatic Co^{2+} effects observed with the undiluted composition, while preserving the beneficial high power effects noted earlier. For the purpose of testing this hypothesis, a series of lithium-titanium ferrite samples of magnetization suitable for X-band microwave phase shifter applications were prepared with Co^{2+} concentrations extending far beyond those of previous investigations.

In this report, the results of peak power and hysteresis loop measurements are presented, and a new model is outlined to explain both the phenomena observed in lithium ferrites and related effects previously reported for Co^{2+} in some garnet lattices.

II. EXPERIMENTAL PROCEDURE

A. Sample Preparation

In order to evaluate the effects of Co^{2+} substitutions in materials designed for actual microwave devices, a polycrystalline lithium-titanium ferrite of 2250 G saturation magnetization ($4\pi M_s$) was chosen. This composition was tailored for X-band phase shifter applications and has the complete chemical formula $\text{Li}_{0.08}\text{Zn}_{0.1}\text{Fe}_{0.82}[\text{Li}_{0.5}\text{Ti}_{0.26}\text{Al}_{0.1}\text{Mn}_{0.05}\text{Bi}_{0.005}\text{Fe}_{1.085}]\text{O}_4$. With

reference to generic lithium ferrite $\text{Fe}[\text{Li}_{0.5}\text{Fe}_{1.5}]\text{O}_4$, it should be noted that the octahedral (B) sites contain, in addition to the principal magnetic dilutant Ti^{4+} , small amounts of Al^{3+} and Mn^{3+} , as well as a trace substitution of Bi^{3+} . The Al^{3+} was added to improve temperature stability, Mn^{3+} to insure good dielectric properties, and Bi^{3+} to control microstructure. In the A sublattice, excess Li^{1+} (required to help offset the charge imbalance caused by B-sublattice Ti^{4+}) is present together with a small amount of Zn^{2+} added to improve hysteresis loop properties. For this study, the small amounts of zinc and aluminum have a slight influence on the magnetic interactions, but the manganese and bismuth can be ignored. For the introduction of Co^{2+} ions to this system, we need only to consider the pertinent elements in the basic formula. In this case, the addition of Co_x to the octahedral sublattice requires that the B-site lithium and iron become $\text{Li}_{0.5-x/2}$ and $\text{Fe}_{1.085-x/2}$ in the formula unit [14].

Materials preparation was carried out by conventional ceramic processing techniques that included powder formation by ball milling and spray drying, and sintering at temperatures below 1050 K to prevent Fe^{2+} ion formation. From the final sintered specimens, rectangular bars, toroids, and spheres were formed to be used for measurements of peak power thresholds and hysteresis loop properties.

B. Measurements

Room temperature measurements of ferrimagnetic resonance and spinwave linewidths were carried out at X-band frequency by means of conventional waveguide experiments, with spinwave linewidths calculated from the usual relation [16]

$$\Delta H_{k \rightarrow 0} = (\gamma 4\pi M_S / \omega) h_{\text{crit}} , \quad (1)$$

where h_{crit} is the minimum critical microwave field intensity for the onset of spinwave instability, ω is the frequency in MHz and γ is the gyromagnetic splitting factor ($= 2.8 \text{ MHz/G}$). In these experiments, the values of ω and $4\pi M_S$ were unchanged for each sample tested, and the relation between peak power and $\Delta H_{k \rightarrow 0}$ was a simple quadratic function. The imaginary part of the permeability μ'' was measured at X-band to monitor the expected increase in magnetic loss.

For latching phase shifter applications, it is desirable for the hysteresis loop to have a high remanent magnetization ($4\pi M_r$) and low coercive force (H_c). Measurements of the hysteresis loop can be carried out with either toroidal or rectangular bar-shaped samples. In this work, bar specimens were used with a high-field hysteresigraph employing a magnetic potentiometer of the type developed by Weiss [17]. Loop parameter data at room temperature were recorded from direct measurements and photographs of the low field portion of the loops were taken from oscilloscope traces.

III. EXPERIMENTAL RESULTS

In Fig. 1, the results of spinwave linewidth measurements at 9.4 GHz are plotted as a function of Co^{2+} concentration, with x values up to 0.05. As anticipated, $\Delta H_{k \rightarrow 0}$ increased linearly from 1.7 to 22.6 Oe over this range of concentrations. Earlier measurements on similar compositions by Green and Van Hook [11], plotted in Fig. 1, also reveal a linear rise in the spinwave linewidth at zero internal field $\Delta H_k (H_i = 0)$. Since this parameter is greater than $\Delta H_{k \rightarrow 0}$, the discrepancy between the two curves is in accord with expectations [16].

Since the spinwave instability threshold power is proportional to the square of $\Delta H_{k \rightarrow 0}$, the peak power is expected to follow a parabolic function (normalized to the power level at $x = 0$) that will increase by a factor of more than 100 over this range, as plotted in Fig. 2. Even for a comparatively modest Co^{2+} substitution of 0.02 ions per formula unit, peak power capability should increase by a factor of almost 40. In Fig. 3, μ'' is plotted as a function of x to show the linear rise in magnetic loss. The small increases above the corresponding earlier data [11] are probably the result of microstructure inhomogeneities. It is also interesting that over the concentration range $0 \leq x \leq 0.05$, both $\Delta H_{k \rightarrow 0}$ and μ'' increase by a similar factor. This result

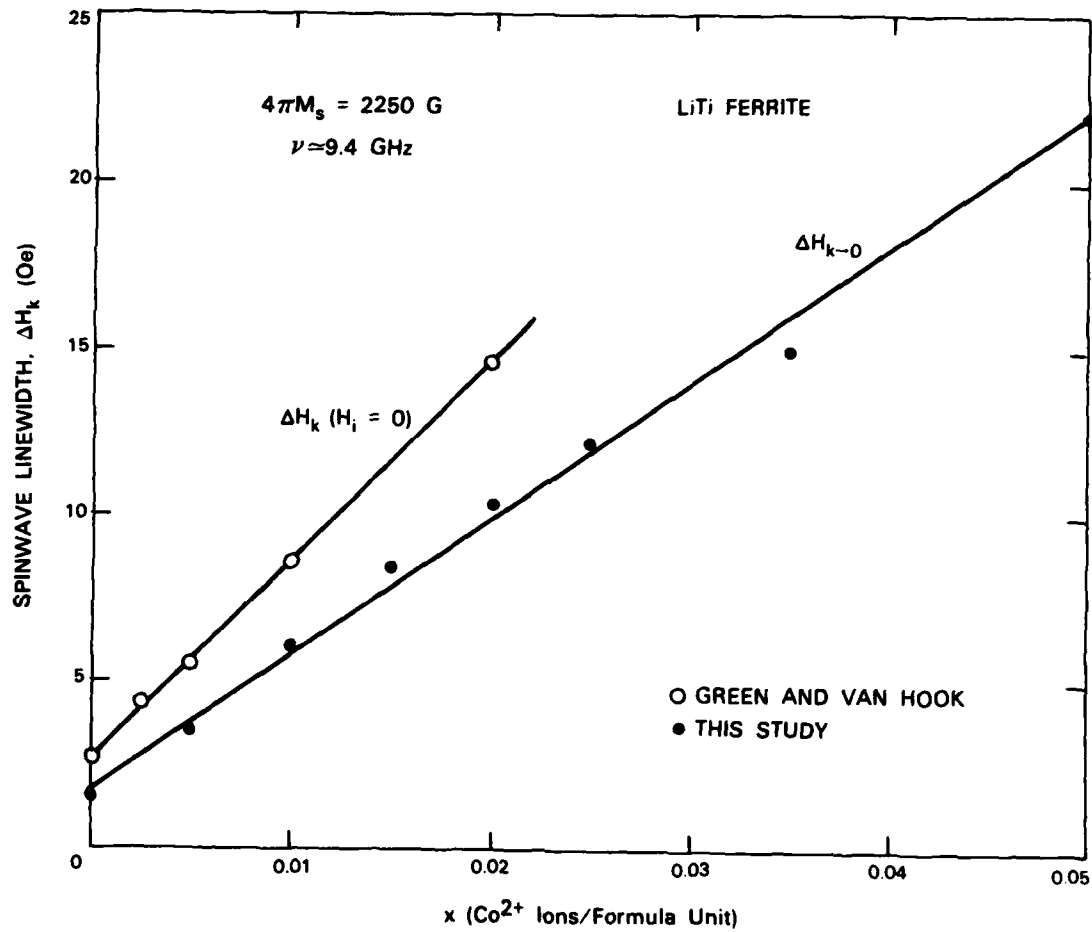
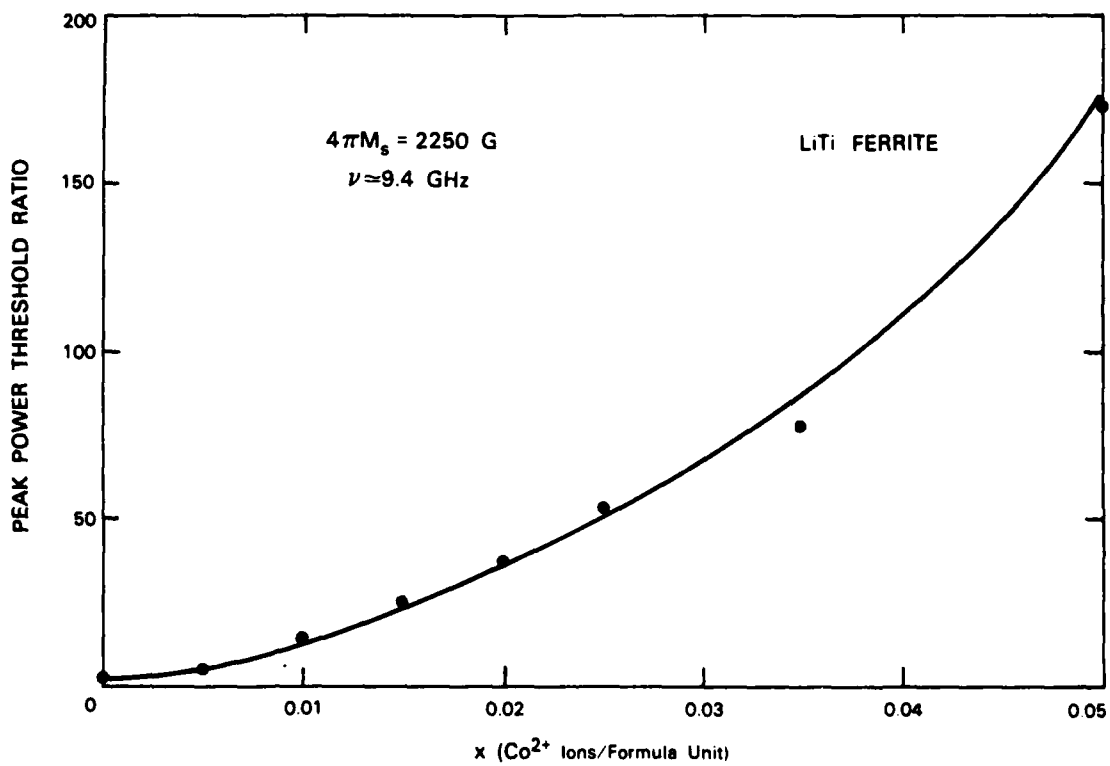


Figure 1. Spinwave linewidth $\Delta H_{k=0}$ as a function of Co^{2+} concentration. Comparison is made with measurements of $\Delta H_k(H_i=0)$ by Green and Van Hook [11].



142087-N

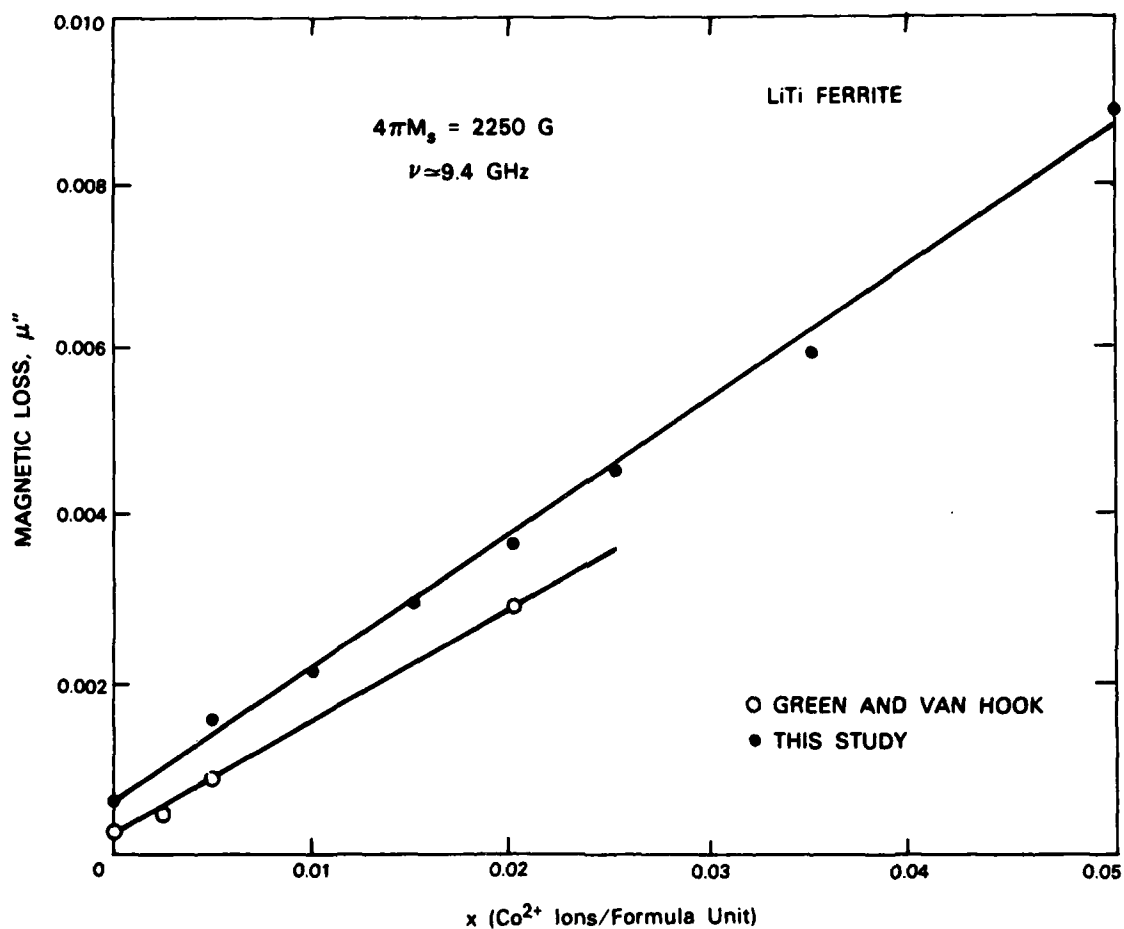
Figure 2. Peak power threshold increase ratio as a function of Co^{2+} concentration.

lends further credence to the theory that both of these parameters depend directly on the Co^{2+} spin-lattice relaxation rate. As indicated in Fig. 4, the resonance linewidth ΔH did not have a minimum value, in agreement with the results of Banerjee et al. [15].

From inspection of the photographs in Fig. 5, it is clear that the hysteresis loop did not suffer the sharp deterioration reported by Van Hook and Dionne for the undiluted composition [13]. In Figs. 6 and 7, the remanence ratios $4\pi M_r/4\pi M_s$ and coercive forces H_c of the samples from the present study are compared with earlier results for the room temperature case. Although the remanence ratios of the Ti^{4+} -substituted samples decreased from about 0.72 to about 0.50 at $x = 0.05$, the remanence ratios of the pure Li ferrite samples fell sharply above $x = 0.01$ to reach almost 0.30 at $x = 0.02$. In the same manner, H_c of the diluted samples rose in a gradual slope from 1.6 to 4.2 Oe over the complete range, while for the undiluted material H_c reached 4.3 Oe on a steep slope at only $x = 0.02$. Based on these data, it may be concluded that the anisotropy cancellation effects normally attributed to Co^{2+} ions do not appear in the samples examined in the present study.

IV. EXCHANGE ISOLATION OF Co^{2+}

To understand the role played by cobalt ions in the magnetic



142088-N

Figure 3. Magnetic loss μ'' (partially magnetized state) as a function of Co^{2+} concentration. Comparison is made with measurements of Green and Van Hook [11].

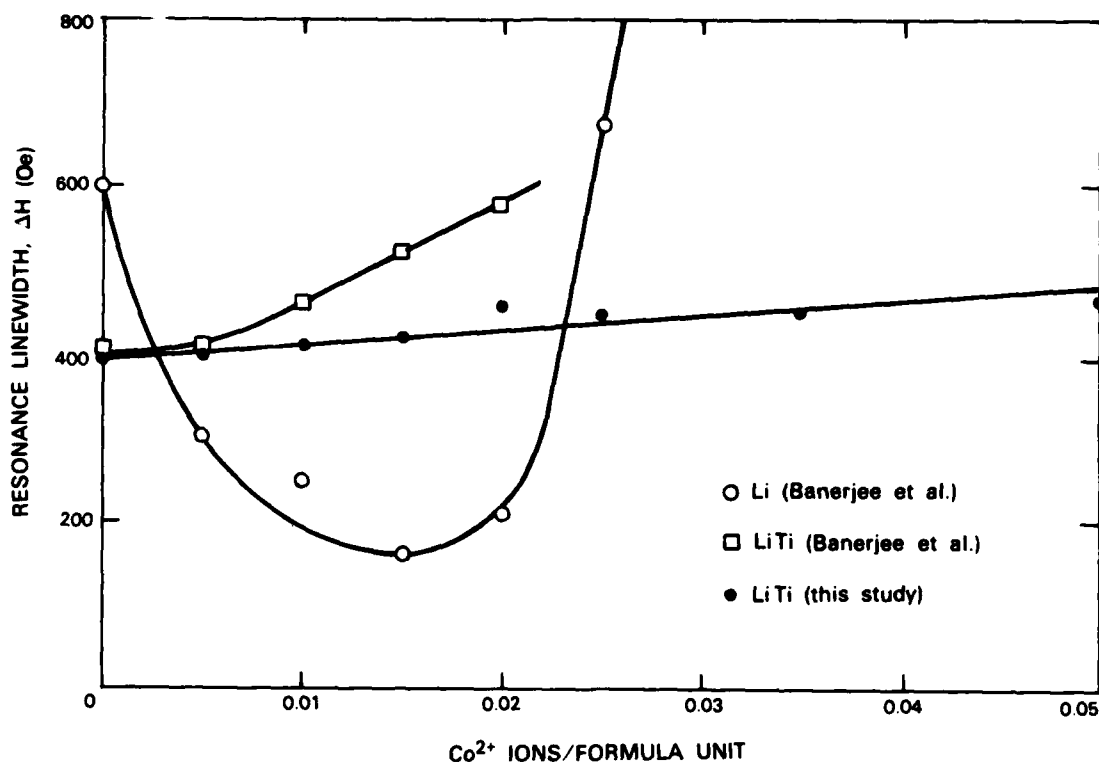


Figure 4. Ferrimagnetic resonance linewidth ΔH as a function of Co^{2+} concentration. Comparison is made with earlier data of Banerjee et al. [15].

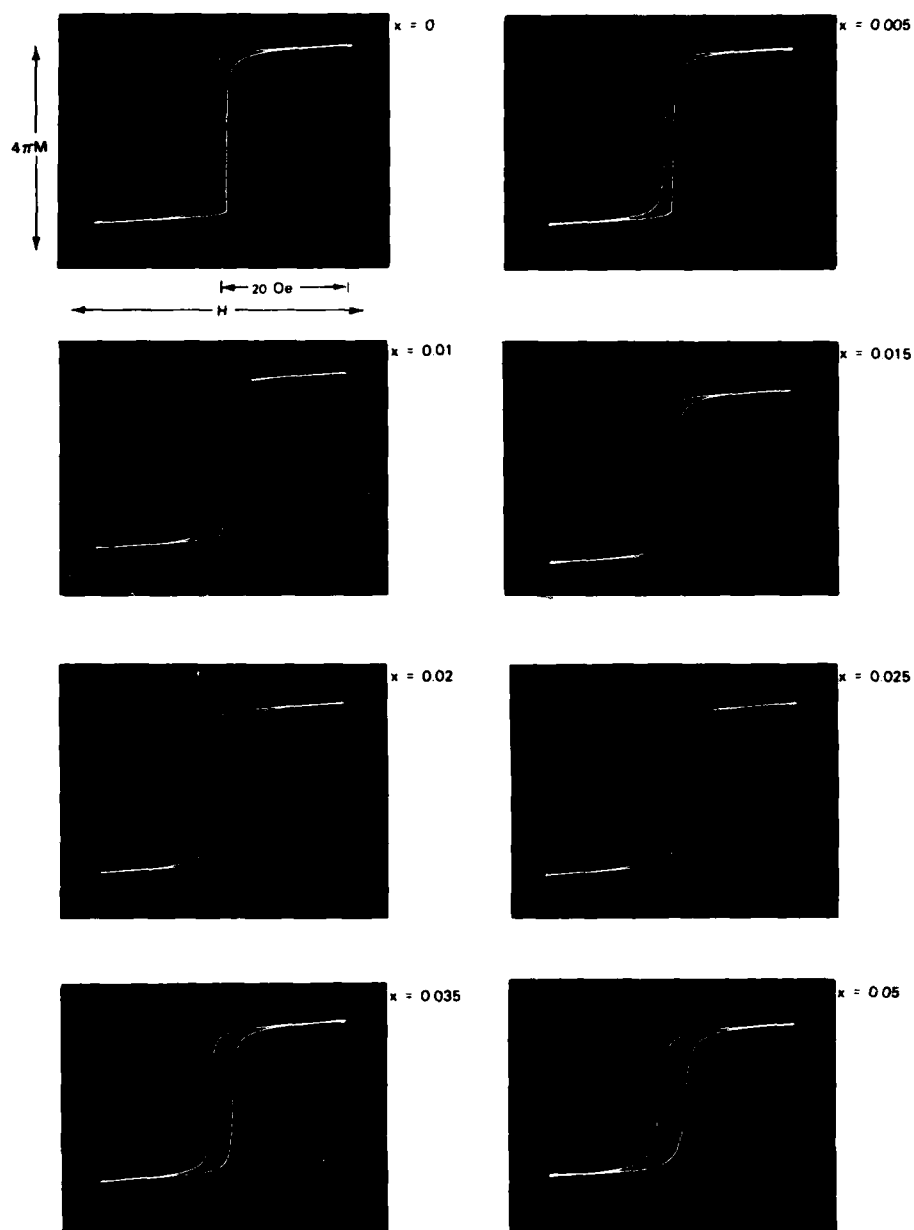


Figure 5. Hysteresis loop photos of the series of LiTi ferrite compositions with x values ranging up to 0.05 ions/formula unit.

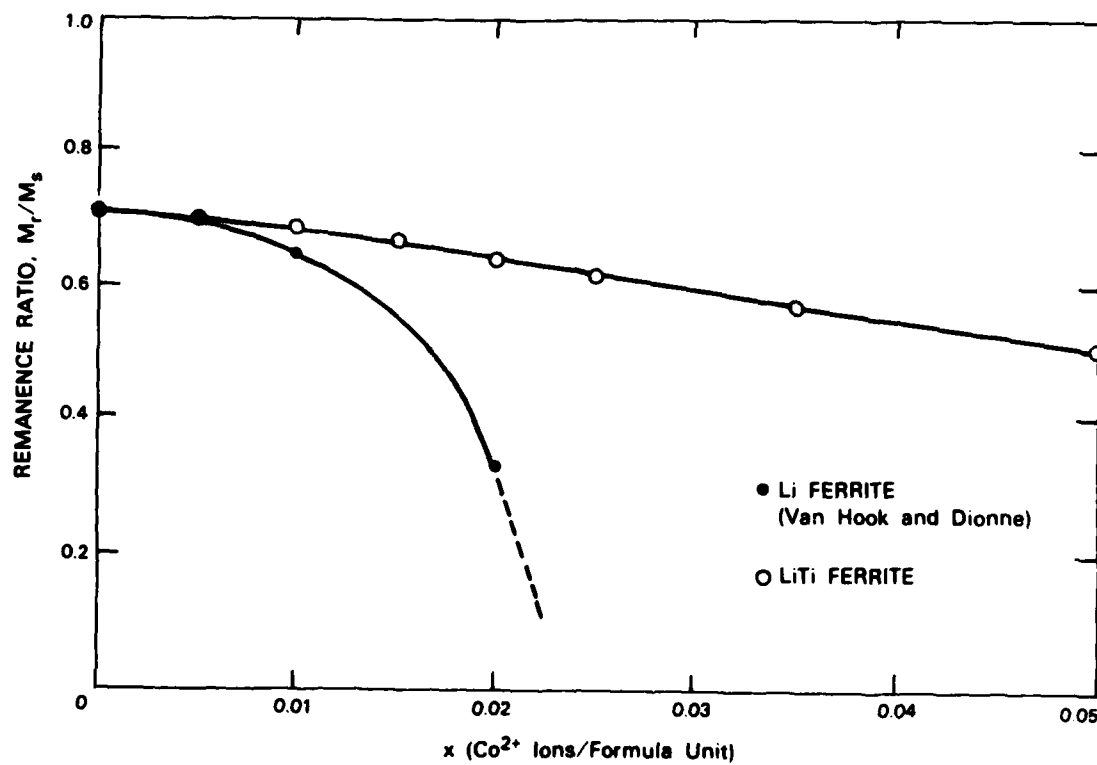


Figure 6. Remanence ratio as a function of Co^{2+} concentration. Comparison is made with earlier data of Van Hook and Dionne [13].

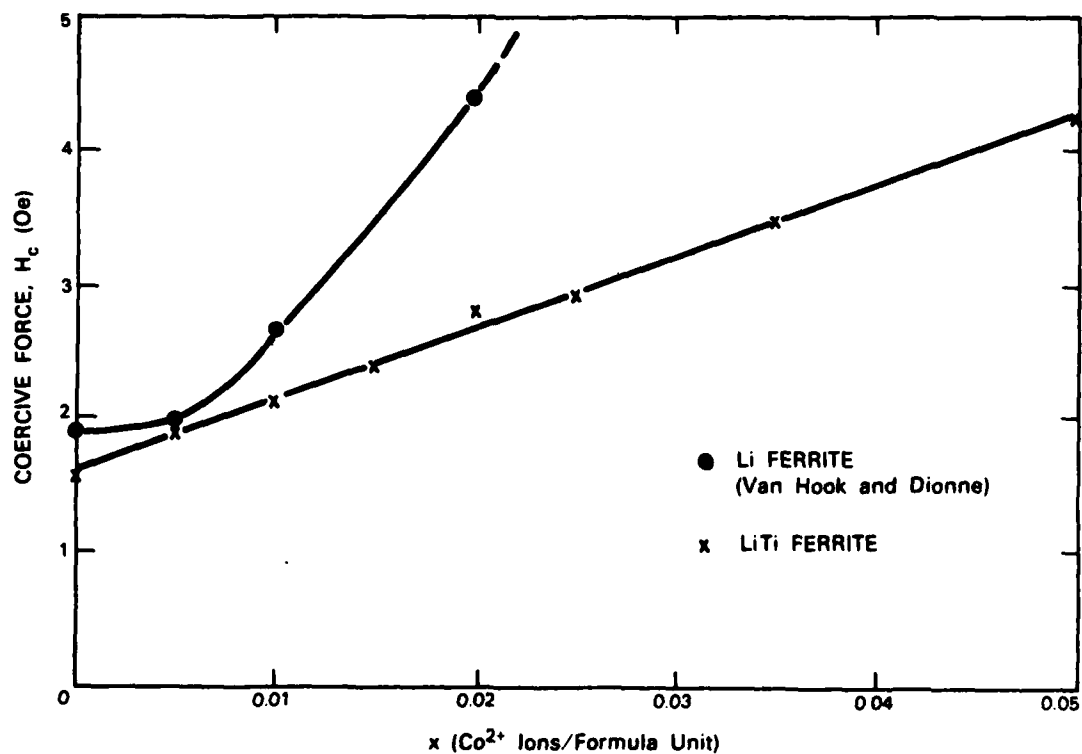


Figure 7. Coercive force as a function of Co^{2+} concentration. Comparison is made with earlier data of Van Hook and Dionne [13].

142092-N

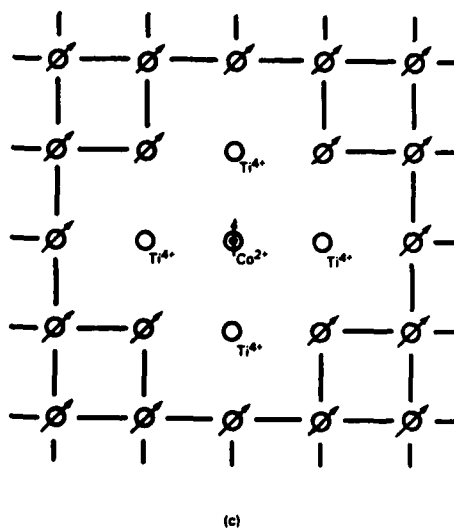
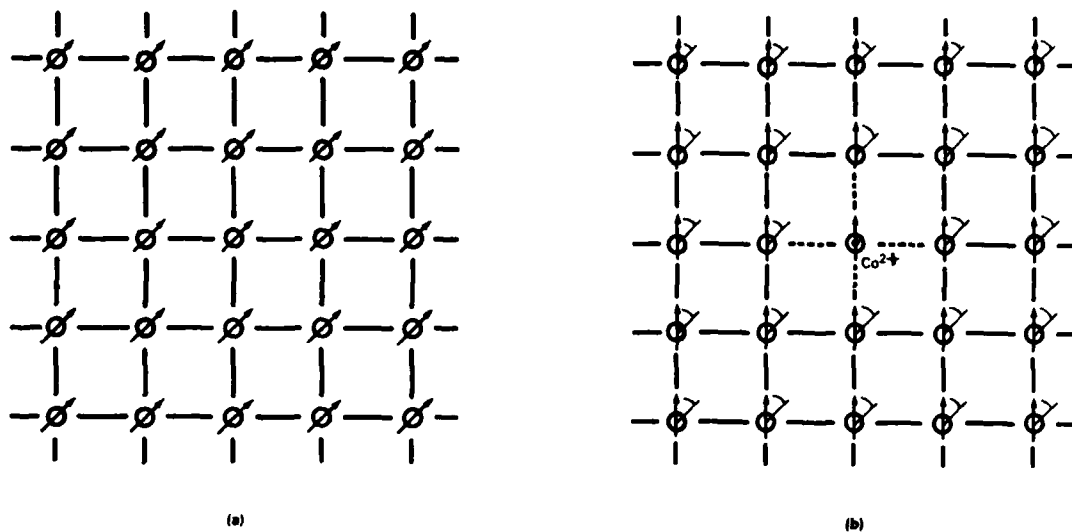
properties of lithium ferrite, it is important to recognize that Co^{2+} differs from Fe^{3+} and Li^{1+} (the ions that it replaces) in several ways. The most obvious change is the ionic charge discrepancy which requires that on the average two Co^{2+} ions replace one Li^{1+} and one Fe^{3+} in octahedral sites. In a stoichiometric system, the Co^{2+} may replace either of these ions with equal probability, causing local changes in the electrostatic and magnetic exchange energies. Perhaps the most noteworthy feature of Co^{2+} is its strongly positive first-order magnetocrystalline anisotropy K_1 , which opposes the normally negative K_1 of the iron sublattices [18]. In addition, Co^{2+} couples ferrimagnetically to Fe^{3+} in both A and B sublattices through strong superexchange interactions [19]. Finally, the Co^{2+} ions provide rapid spin-lattice relaxation paths for the Fe^{3+} spin system through both short range exchange and longer range dipolar couplings.

To explain why the addition of cobalt to the lithium-titanium ferrite composition failed to cause changes in K_1 , it was originally thought that the Ti^{4+} ions altered the crystal field energy level structure of Co^{2+} [15]. Other possibilities would be that the cobalt entered tetrahedral sites or changed valence states. Because the fast relaxation seen in the $\Delta H_{k \rightarrow 0}$ data of Fig. 1 is characteristic of octahedral-site Co^{2+} ions with degenerate orbital ground states, however, none of these mechanisms

can completely solve this paradox.

As a consequence, we must now consider the possible changes in the Co^{2+} environment introduced by the presence of clustered dilutants as modeled in Fig. 8. Co^{2+} in octahedral sites will make large positive contributions to the normally negative anisotropy of the iron sublattices [18]. This phenomenon is considered to be largely "single-ion" in nature and should be viewed as localized when the cobalt concentrations are too small to produce cooperative effects. At this point, it is important to note that the Co^{2+} anisotropy can be communicated to the iron sublattices only through magnetic superexchange interactions with nearest neighbor Fe^{3+} ions in A and B sites. As depicted in Fig. 8, the Co^{2+} spin favors a direction different from the normal easy axis and is capable of causing a rotation of the surrounding Fe^{3+} spins through strong exchange interactions. If sufficient non-magnetic ions cluster about the Co^{2+} and decouple it from the iron sublattice exchange field, the iron sublattice would return to its normal easy direction. Thus, without the exchange couplings J_{AC} and J_{BC} depicted by the three-ion model in Fig. 9, the individual Co^{2+} anisotropy effects would be decoupled from the rest of the lattice and would be virtually undetected at the small concentrations considered in this study. In effect, Co^{2+} would behave as a paramagnetic ion, coupled to the Fe^{3+} only through dipolar fields.

142093-N
142094-N



142095-N

Figure 8. Two-dimensional exchange isolation model for a single sublattice: (a) normal Fe^{3+} occupation with diagonal easy axis of magnetization, (b) rotation of Fe^{3+} spins through exchange coupling to single Co^{2+} ion with vertical easy axis, and (c) Fe^{3+} spins return to diagonal axis when Ti^{4+} dilutants decouple Co^{2+} from the exchange field.

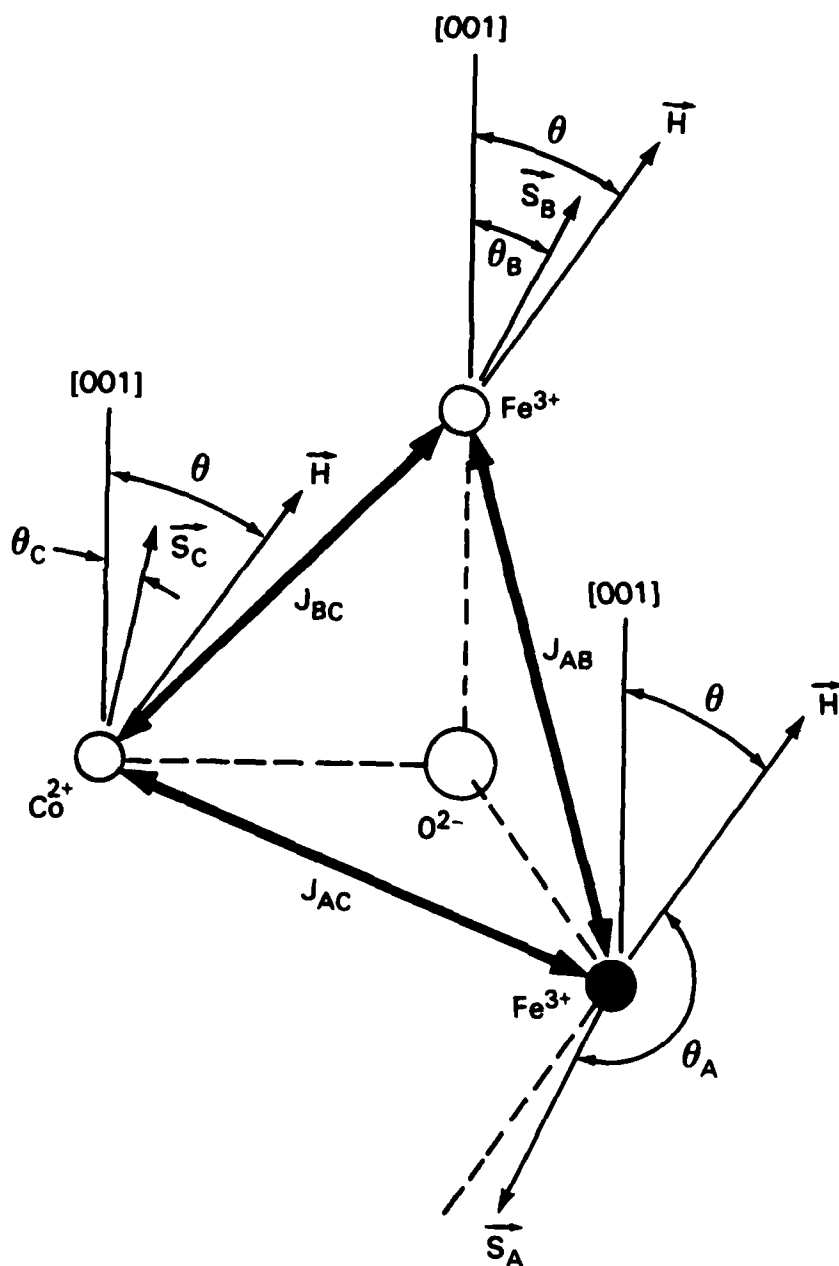


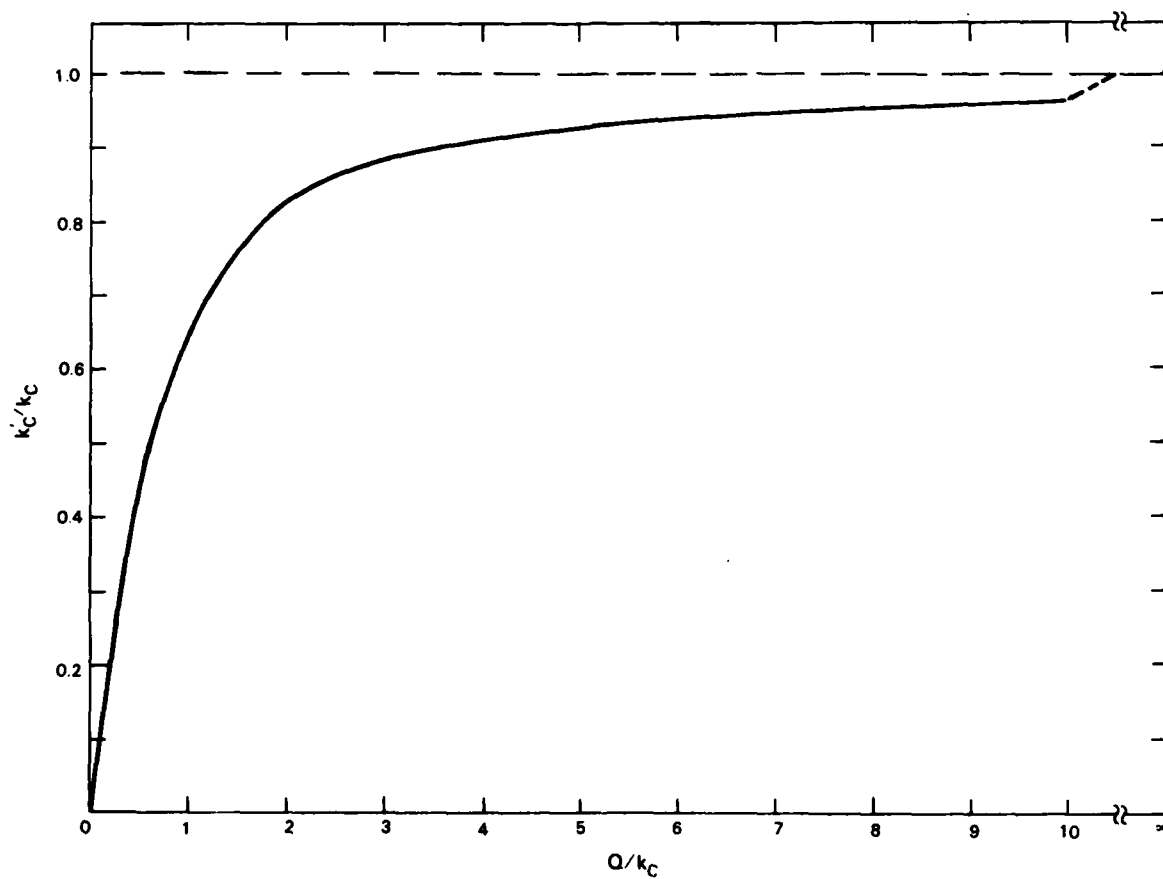
Figure 9. Three-ion approximation to spinel cation exchange interactions.

From the analysis of the three-ion model presented in Appendix A, it is shown by Fig. 10 that a reduction in the exchange energy parameter Q will cause a decrease in the effective anisotropy contribution k_C' . According to Slonczewski [18], the exchange energy for magnetite is about 600 cm^{-1} , while the single ion anisotropy k_C of Co^{2+} was measured as 2.5 cm^{-1} at 300 K. Since the shape of the curve suggests that k_C'/k_C would not become small until $Q/k_C < 1$, the isolation effect may not occur in this system until all of the exchange couplings have been removed by nonmagnetic substitutions.

As indicated by the spinel octahedral site exchange couplings shown in Fig. 11, there are six principal B-site and six A-site nearest neighbor cations surrounding the Co^{2+} ion. From earlier work on this system [20], it was determined that $|J_{AB}| > |J_{BB}|$ for Fe^{3+} ions. This inequality will also apply to the $\text{Co}^{2+}-\text{O}^{2-}-\text{Fe}^{3+}$ exchange, but with smaller constants because of the unmatched cations [19]. For complete magnetic exchange isolation to occur, all twelve of these Fe^{3+} ions would have to be replaced by nonmagnetic substitutes, and for significant partial isolation, at least the six A-sites would have to be diluted.

V. CATION CLUSTERING MECHANISMS

In considering the three systems discussed in the Introduction, (Li ferrite, LiAl ferrite, and LiTi ferrite), only the last



142097-N

Figure 10. Effective Co²⁺ anisotropy constant k_C' as a function of the exchange coupling parameter Q , expressed as ratios of k_C .

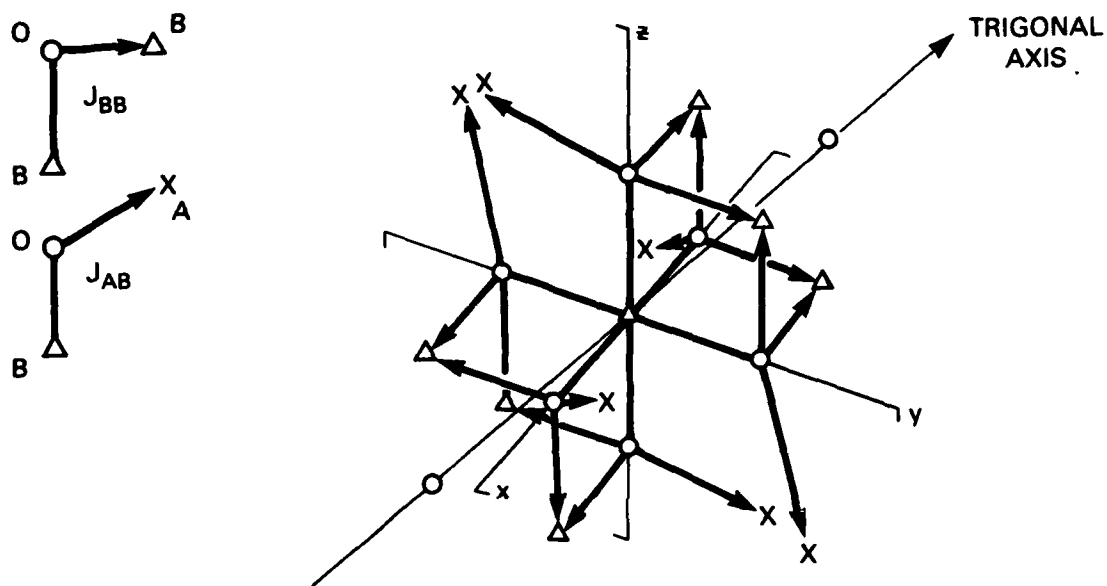


Figure 11. Partial unit cell of spinel lattice surrounding an octahedral (B) site. Superexchange couplings are indicated between neighboring cations.

contains nonmagnetic (Li^{1+}) ions in the A sublattice*. It is evident, however, that the amounts present even in compositions with quite large concentrations of Ti^{4+} are insufficient to reduce significantly the J_{AC} of the system, unless there is a preferential distribution of Li^{1+} in the A sites adjacent to the Co^{2+} ions. To explain how such an excess of dilutant would cluster about cobalt sites, three mechanisms are proposed: exchange energy minimization, lattice electrostatic energy optimization, and crystal field energy stabilization.

A. Magnetic Exchange Energy

In general, magnetic exchange forces will tend to oppose reordering of Fe^{3+} ion couplings wherever dilutants are introduced. The greater the number of exchange couplings, the lower the system free energy will be. For this reason, magnetic inhomogeneities in the form of nonmagnetic second phase on a molecular scale are quite common in ferrites with sizeable concentrations of dilutants [21-23], particularly where competing charge compensation requirements are not present.

When a pair of Co^{2+} ions replace a $\text{Li}^{1+}\text{-Fe}^{3+}$ combination, local charge imbalances may occur if adjustments are not made in

*The addition of Zn^{2+} ions will also dilute the A sublattice. Their effect on magnetization and anisotropy is examined in Appendix D.

the adjacent cation sites. For example, where Co^{2+} replaces Li^{1+} , an excess positive charge is introduced and compensation can be obtained only by other Li^{1+} ions migrating to the neighboring B sites; where Co^{2+} replaces Fe^{3+} , it is Fe^{3+} migration that must do the charge compensation. In this latter situation, the migration of Fe^{3+} tends to destabilize the net exchange energy because of the reduction in the number of Fe^{3+} mutual superexchange couplings. Where Ti^{4+} is introduced as a dilutant to B sites and excess Li^{1+} to A sites, however, a more efficient compensation scheme becomes available. By preferential clustering of Ti^{4+} and Li^{1+} in the B and A sites respectively surrounding the Co^{2+} ions, not only are the local electric field energies minimized at nearest neighbor sites in both sublattices, but the Fe^{3+} ions are freed to form a maximum number of $\text{Fe}^{3+}-\text{O}^{2-}-\text{Fe}^{3+}$ superexchange couplings throughout the rest of the lattice. This latter mechanism would serve to stabilize the exchange field energy because the mutual Fe^{3+} couplings are expected to be stronger than those of the $\text{Co}^{2+}-\text{O}^{2-}-\text{Fe}^{3+}$ combinations mentioned earlier.

B. Lattice Electrostatic Energy

In early work carried out on spinels, Verwey and his co-workers investigated the cation site distribution from the standpoint of electrostatic energy [24,25]. In particular, they

determined that normal spinels, $A^{2+}[B^{3+}_2]O_4$ in general have larger Madlung constants than inverse spinels, $A^{3+}[B^{2+}B^{3+}]O_4$. From their calculations, which were found to be in reasonably good agreement with x-ray crystallographic data, they established general rules governing the site preference of various ions based on electrostatic considerations. Their conclusion most relevant to the problem at hand is that normal spinels tend to have larger Madlung constants (i.e. greater electrostatic stability) where higher valence cations occupy sites of higher oxygen coordination. Thus, for maximum electrostatic stability, the monovalent and divalent cations should occupy tetrahedral sites and the trivalent and tetravalent ions, the octahedral sites.

Without the influence of magnetic exchange energies which dictate Fe^{3+} ions in tetrahedral sites, as is the case of most iron-bearing spinels, the generic $Fe[Li_{0.5}Fe_{1.5}]O_4$ would more likely be $Li_{0.5}Fe_{0.5}[Fe_2]O_4$, with only Fe^{3+} in octahedral sites. If this exercise is carried a step further by replacing all of the Fe^{3+} with Co^{2+} - Ti^{4+} combinations, the fictitious compound would then take the form of $Li[Co_{0.5}Ti_{1.5}]O_4$. In this situation, the Co^{2+} of necessity would be surrounded by only nonmagnetic Li^{1+} in A sites and by nonmagnetic Ti^{4+} in three out of four B sites (see Fig. 11). Since the Madlung constant for this hypothetical composition would be greater than that of $Fe[Li_{0.5}Fe_{1.5}]O_4$, it is not unreasonable to expect that cation

- O^{2-}
- X A ION
- △ B ION

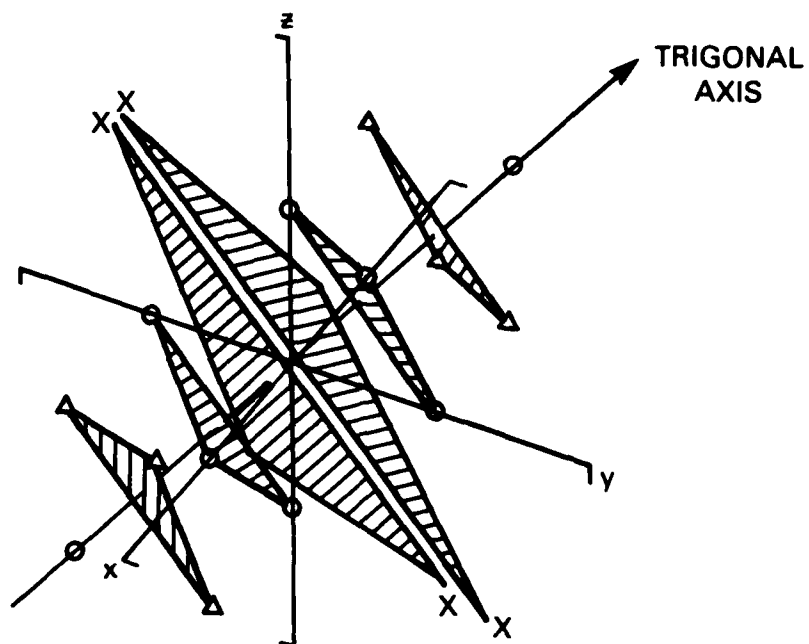


Figure 12. Origin of the octahedral-site crystal field, indicated by triangles of ligands about $[111]$ axis of symmetry.

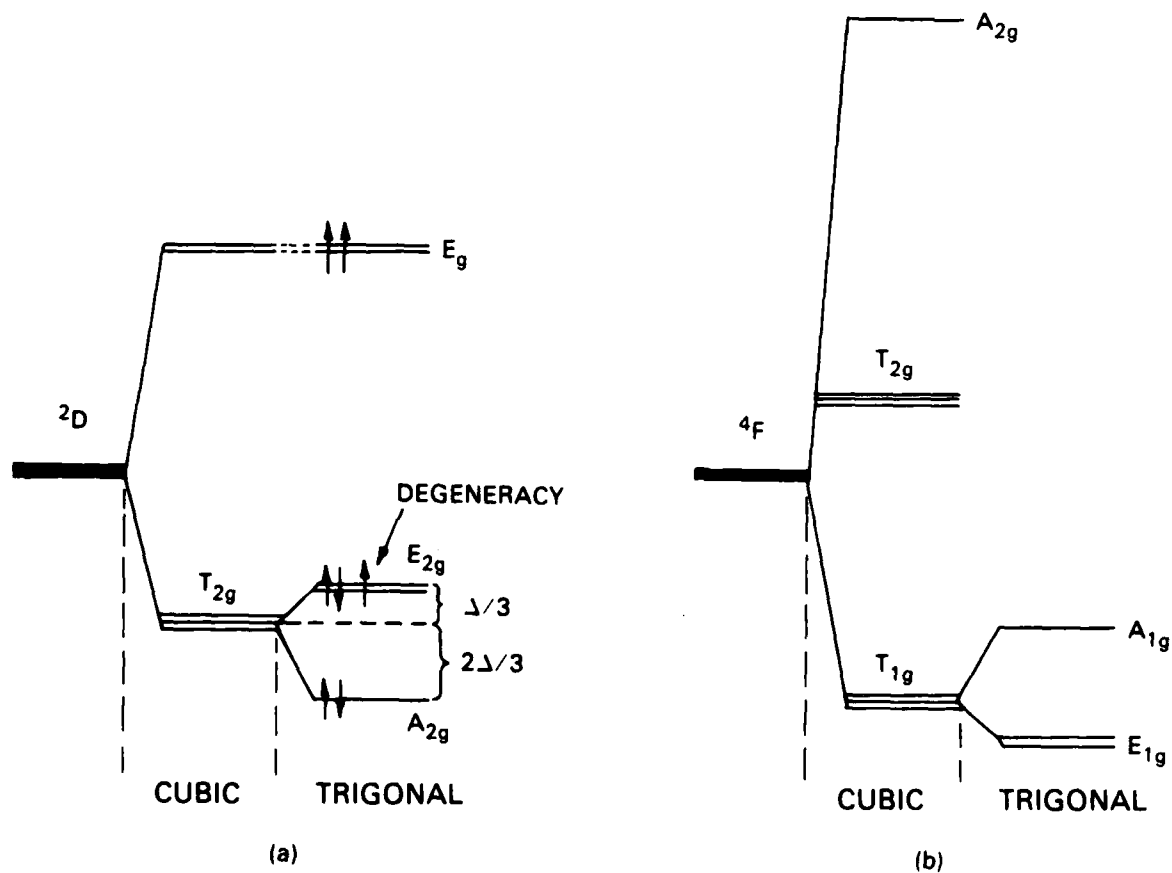


Figure 13. Crystal field energy level diagrams for Co^{2+} : (a) single d-electron model for a high-spin ($S=3/2$) d^7 configuration, and (b) energy levels for an $4F$ -state (d^7) ion.

142100-N

distributions similar to the above would be established locally about the sites occupied by Co^{2+} ions. In this manner, electrostatic energy stabilization would be enhanced by the $\text{Li}^{1+}\text{-Ti}^{4+}$ occupation of nearest-neighbor cation sites surrounding Co^{2+} , and all Co^{2+} superexchange interactions with Fe^{3+} would be removed.

C. Crystal Field Stabilization Energy

A third and possibly the most compelling reason why Co^{2+} ions become magnetically isolated from Fe^{3+} in LiTi spinel ferrites may be found in an examination of the static crystal electric field effect on the Co^{2+} ions. In Fig. 12, a model of the ionic distribution surrounding an octahedral site is sketched to illustrate the origin of an axial field component directed along a trigonal axis. For a Co^{2+} ion in this environment, the crystal field stabilization can be determined by inspection of the single d-electron orbital energy level model shown in Fig. 13a, for an octahedral site with a positive trigonal field component. According to Orgel [26], an energy stabilization is expected whenever the combined electron energies are reduced by the energy level splitting. With seven d electrons, Co^{2+} would have both an additional energy stabilization of $\Delta/3$ and a doublet ground state from the trigonal field component. The actual energy level diagram for a d^7 ion with 4F ground term is shown in Fig. 13b, where the orbital degeneracy is indicated.

The order of the energy levels of Co^{2+} in this environment can be determined from inspection of the d-orbital wave function lobes shown in Fig. 14. The lower triplet T_{2g} of Fig. 13 is composed of t_{2g}^0 , t_{2g}^+ , and t_{2g}^- , with only t_{2g}^0 having a lobe directed along the trigonal axis. If the various ions deployed about this axis produce a resultant positive field, t_{2g}^0 would represent a lower energy state, while t_{2g}^+ and t_{2g}^- would be degenerate and of higher energy (see Appendix C). As shown in Fig. 12, the trigonal crystal field is determined by the negative charges of the O^{2-} octahedron, and by the positive charges of the six B ions at corners of the cubes surrounding the body diagonal and the six A ions close to the plane normal to this axis. If the O^{2-} octahedron is not distorted, any axial symmetry components must arise from the locations and charges of the A and B cations. Based on the relative positions of the A and B neighbors, the cation array would be expected to provide a net positive field at the Co^{2+} site and produce a doublet orbital ground state.

For most spinels, the O^{2-} octahedron is not regular, but has a distortion along the diagonal caused by a uniform expansion of the O^{2-} ions that form tetrahedra about the A sites. These displacements in turn create trigonal extensions of the O^{2-} octahedra characterized by the oxygen parameter u , which usually exceeds the ideal value of 0.375 and provides a negative field

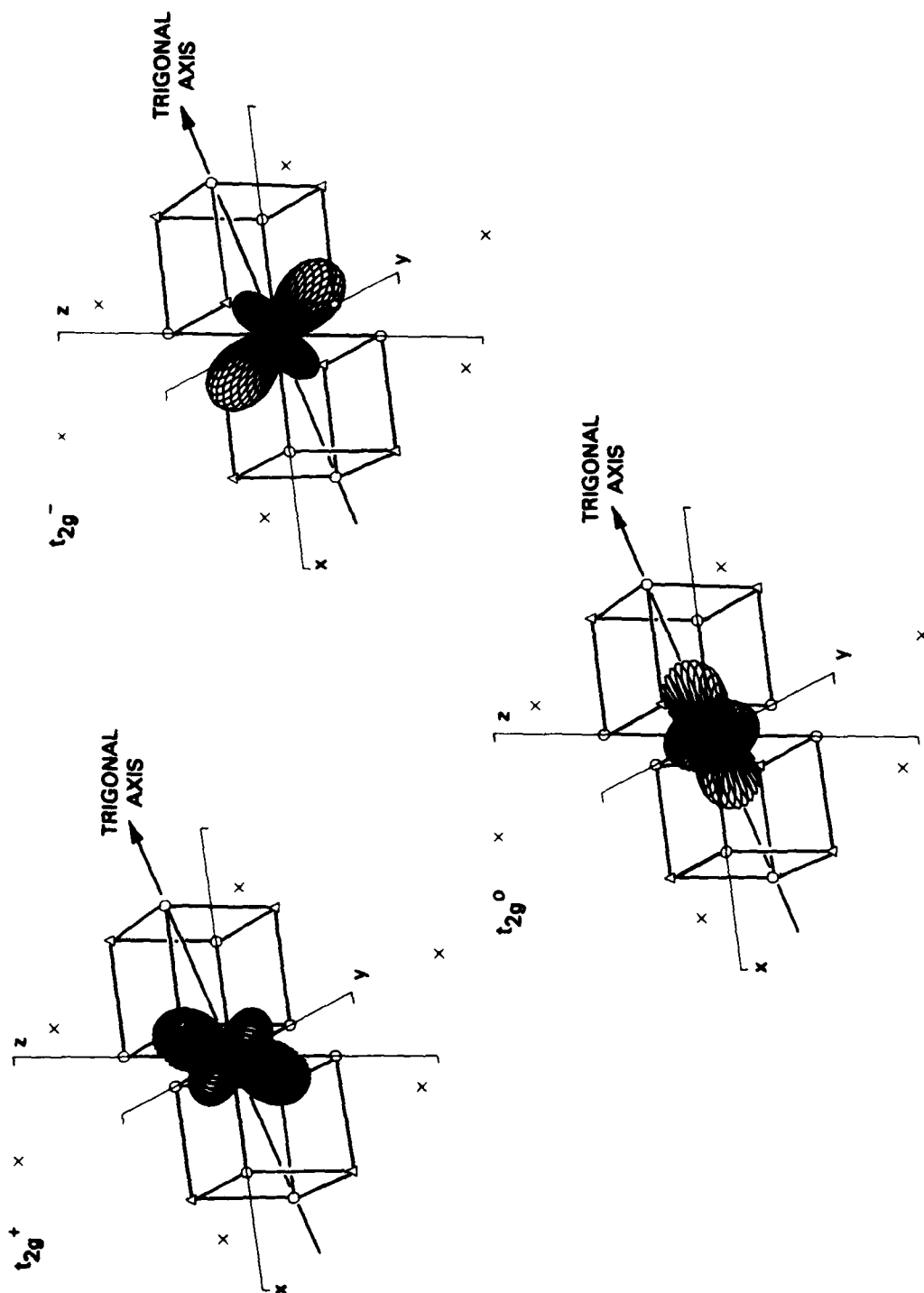


Figure 14. Three-dimensional graphics of T_{2g} orbitals in trigonally distorted octahedral crystal field.

component. Based on this reasoning, a typical B site would thus experience a reduced positive trigonal field that is the resultant of positive and negative components. The relative magnitudes of octahedral distortions may then be estimated from the respective oxygen parameters.

According to the results of the crystallographic analysis presented in Appendix B, u should decrease locally from the experimental value of 0.382 for $\text{Li}_{0.5}\text{Fe}_{2.5}\text{O}_4$ to approximately 0.376 with the larger Co^{2+} ion in the B site and Li^{1+} ions in the surrounding A sites. Under these conditions, the negative trigonal field from distorted octahedra in the host structure would be reduced substantially at this site and the positive trigonal field from the neighboring cation sites would then have its full effect. With Li^{1+} and Ti^{4+} as the respective A and B neighbors, there would be a further increase in the strength of the net positive trigonal field, because the charges of the B ions near the symmetry axis would increase from $1+$ or $3+$ to $4+$, while those of the more distant and nearly orthogonal A cations would reduce from $3+$ to $1+$.

Evidence of enhanced crystal field distortion in LiTi ferrite was reported in the work by Banerjee et al. [15] from Mossbauer effect measurements of the electric quadrupole splitting of B-site Fe^{3+} ions. The fact that the apparent trigonal field increase occurred with normal Li^{1+} - Ti^{4+} distribution

(there was no cobalt in these samples) lends additional support to the argument for strong positive crystal field at the Co^{2+} sites. Under these conditions, the d-electron energy level structure would be expected to agree with Fig. 13, and an enhanced $\Delta/3$ stabilization of the Co^{2+} complex from $\text{Li}^{1+}\text{-Ti}^{4+}$ clustering would increase the likelihood of exchange isolation.

VI. DISCUSSION AND CONCLUSIONS

Based on the experimental findings for hysteresis loops of this heavily Co^{2+} -substituted LiTi ferrite system, it may be concluded immediately that substantial concentrations of Co^{2+} may be used without fear of large changes in the remanence ratio or coercive force at room temperature. It is also apparent that both ΔH_{k+0} and μ'' at X-band continue on linear curves for Co^{2+} concentrations up to 0.05 ions per formula unit. Since both of these parameters depend directly on the spin-lattice relaxation of Co^{2+} , it is not surprising to find that ΔH_{k+0} and μ'' each increase by more than a factor of 10 over this concentration range. The peak power threshold, however, is a quadratic function of ΔH_{k+0} and will increase by a factor greater than 10^2 , thus providing a powerful method for raising peak power limits of microwave devices without dramatic increases in magnetic loss.

With regard to the proposed magnetic exchange isolation model for Co^{2+} in LiTi ferrite, the data reported here will be

examined along with previously published results related to this topic. The effects on anisotropy and hysteresis loops will be discussed first, followed by relaxation phenomena, and finally, by a brief review of Co^{2+} effects in the garnet lattice.

A. Anisotropy and Hysteresis Loops

Because of the unavailability of single crystals of lithium ferrite with large titanium substitutions, most of the evidence related to magnetocrystalline anisotropy for this family must be inferred from polycrystalline specimens, through either ferrimagnetic resonance linewidth or hysteresis loop parameter measurements.

In Fig. 15, the linewidth results of Co^{2+} doping in nickel ferrite [9] and lithium ferrite compositions [15] are plotted. According to the theories of ferrimagnetic resonance line broadening [27], the polycrystalline linewidth is believed to depend principally on a term directly proportional to the magnitude of K_1 or K_1^2 and a second term the proportional to the effective porosity. As seen in these curves, the linewidths reach minimum values at different levels of Co^{2+} in all cases except those of the titanium-substituted compositions. This result strongly suggests that K_1 passes through zero in the compounds that show a minimum in their curve. The residual linewidths at the minima are caused mainly by the porosity terms and to a lesser extent by

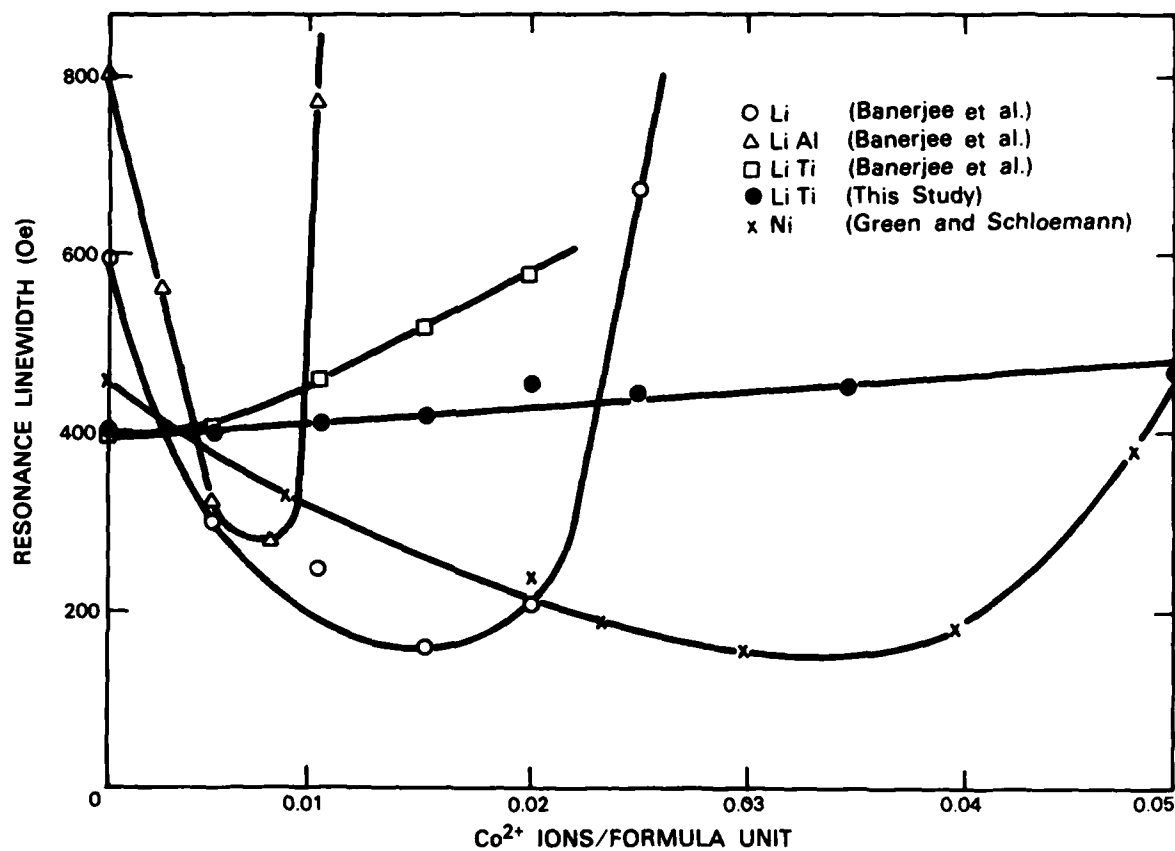


Figure 15. Comparison of Co^{2+} effects on resonance linewidth ΔH among data of present study, Banerjee et al. [15] for Ti^{4+} and Al^{3+} dilutants, and Green and Schloemann for Ni ferrite [9].

intrinsic relaxation phenomena.

As mentioned earlier, the anisotropy compensation value of $x_c = 0.015$ for pure Li ferrite was confirmed by single crystal measurements [14]. With Al^{3+} ions as the dilutant, the compensation value fell to $x_c = 0.007$, in accord with the notion that this trivalent ion will replace Fe^{3+} ions in mainly B sites and will have little effect on either electrostatic energy or crystal fields. As a result, Al^{3+} will reduce directly the negative K_1 produced mainly by the Fe^{3+} ions in the B sublattice and allow the Co^{2+} positive K_1 to compensate the total anisotropy at a lower value of x . For the case of nickel ferrite, compensation occurs at $x_c \approx 0.03$ and is consistent with the higher negative K_1 value for this family, which may arise from the fact that Ni^{2+} ions provide additional magnetic moments to the B sublattice and give rise to a greater dipolar contribution to its anisotropy.

With the LiTi ferrite compositions, decoupling of cobalt from the exchange field is strongly suggested, as there are clearly no minima in the linewidth curves, and consequently no evidence of anisotropy cancellation. The increase in ΔH with x is caused by the intrinsic relaxation of Co^{2+} , which should vary directly with cobalt concentration and inversely with magnetization [28,29]. This latter dependence could account for the increased slope for the new results, since the magnetization of the sample studied in this work was more than double that of the

earlier composition [15].

The hysteresis loop parameters for the compositions of this current study also point to the presence of cobalt exchange isolation. The results plotted in Figs. 6 and 7 reveal that anisotropy cancellation effects from Co^{2+} in a LiTi ferrite composition do not occur up to $x = 0.05$. Where K_1 reverses sign, it is expected that regions of large positive K_1 in the neighborhood of the Co^{2+} ions would lead to large local domain wall energies that would in turn cause large coercive forces when walls are pinned on pores, grain boundaries, or regions of nonmagnetic phase. In addition, nucleation of reverse domains would occur earlier in the switching cycle and large positive K_1 values would be expected to produce even larger spike domains [30]. These effects would cause severe reductions in the remanent magnetization of the type reported earlier by Van Hook and Dionne [13] for pure lithium ferrite. For this host composition, the presence of a small amount of Al^{3+} should have an effect similar to that described above, while the Zn^{2+} substitution in the A sublattice (see Appendix D) would serve to promote exchange isolation by reducing the number of critical J_{AC} couplings to Co^{2+} . It is perhaps this effect that occurred in the recent experiments of Beuzelin et al. with Co^{2+} in LiZn ferrite [31].

B. Relaxation Effects

Because the Co^{2+} ion is believed to have a degenerate orbital ground state in octahedral O^{2-} complexes, its spin-lattice relaxation rate is high in comparison with most of the iron group transition metal ions ($3d^n$). This relaxation effect is enhanced further by the relatively large spin-orbit coupling constant λ of Co^{2+} , which can influence the relaxation rate through a factor related to $(\lambda/\Delta')^4$ in only the direct process [32]. Even in situations where the orbital ground state is nondegenerate, modest values of the orbital energy level splitting Δ' can still account for rapid relaxation rates, regardless of sign.

In ferrite materials at microwave frequencies, the relaxation properties of Co^{2+} are manifested through $\Delta H_{k \rightarrow 0}$ and the imaginary part of the complex permeability μ'' . Both of these quantities are directly related to the spin-lattice relaxation rate. From the results for $\Delta H_{k \rightarrow 0}$ plotted in Fig. 1, which are in general agreement with those of Green and Van Hook [11], and Baba et al. [3], it is clear that Co^{2+} retains its relaxation properties in spite of the apparent exchange isolation in the presence of Ti^{4+} substitutions.

To explain how this effect can occur, one need only to recall that dipolar interactions can easily serve as the vehicle for transmitting energy from the Fe^{3+} spin system to the

individual Co^{2+} relaxation centers. Superexchange couplings are short-range interactions, but dipolar effects are longer range and have been invoked to explain paramagnetic resonance linewidth broadening and a variety of cross relaxation phenomena involving fast-relaxing ions [33]. As a consequence, it should not be surprising to find that anisotropy effects may be eliminated through removal of local exchange couplings without a major change in the relaxation behavior of these compositions.

Based on the results of earlier theoretical work [28,29] and previous measurements of the effects of fast-relaxing ions in ferrites [34,35], the linear dependence of ΔH_{k+0} on cobalt concentration is in accord with expectations. The spinwave linewidth is a direct measure of the spin-lattice transition probability [9,34] and would be proportional to the number of isolated relaxation centers, wherever the relaxation rates of these ions far exceed that of the Fe^{3+} ions in the host lattice.

C. Cobalt Effects in Garnets

Although the major interest of this work has been the Co^{2+} effects in spinel lattices, it is important that the exchange isolation model be examined in relation to the garnet lattice where similar anisotropy effects have been reported. Anisotropy reversal effects were reported for Co^{2+} in $\text{Y}_3\text{Fe}_5\text{O}_{12}$ single crystals by Dionne and Goodenough [5]. In addition, linewidth minima

from Co^{2+} in polycrystalline specimens of garnets with Ca^{2+} and V^{5+} substitutions were found by Llabres et al. [6] and some of their results are reproduced in Fig. 16. The relaxation effects of cobalt in garnets were observed by Krishnan as a ΔH -broadening in single crystals [7]. From the evidence available, it appears that the Co^{2+} ions in octahedral sites of garnet lattices produce anisotropy and spin-lattice relaxation effects very similar to those of spinels.

As shown in Fig. 17, the neighboring ions of an octahedral (a) site in the garnet structure form trigonal arrays about a $\langle 111 \rangle$ axis, similar to the spinel case in Fig. 11. In most cases, the garnet O^{2-} octahedra are not distorted to the same extent as those of the spinels and are not likely to provide strong trigonal field components. Another crystallographic difference lies in fact that a-site ions do not contribute appreciably to this axial field component. It is the dodecahedral c-site ions that are stationed about the symmetry axis, while tetrahedral d-site ions occupy near-orthogonal positions.

Unlike spinels, garnets require an average cation valence of 3+ in each site. With most standard dilution schemes, trivalent ions are used to replace Fe^{3+} and charge balance or crystal field stabilization are not expected to be altered. When Co^{2+} is substituted, the compensating amounts of either Si^{4+} or Ge^{4+} in tetrahedral sites should have only a small perturbation on

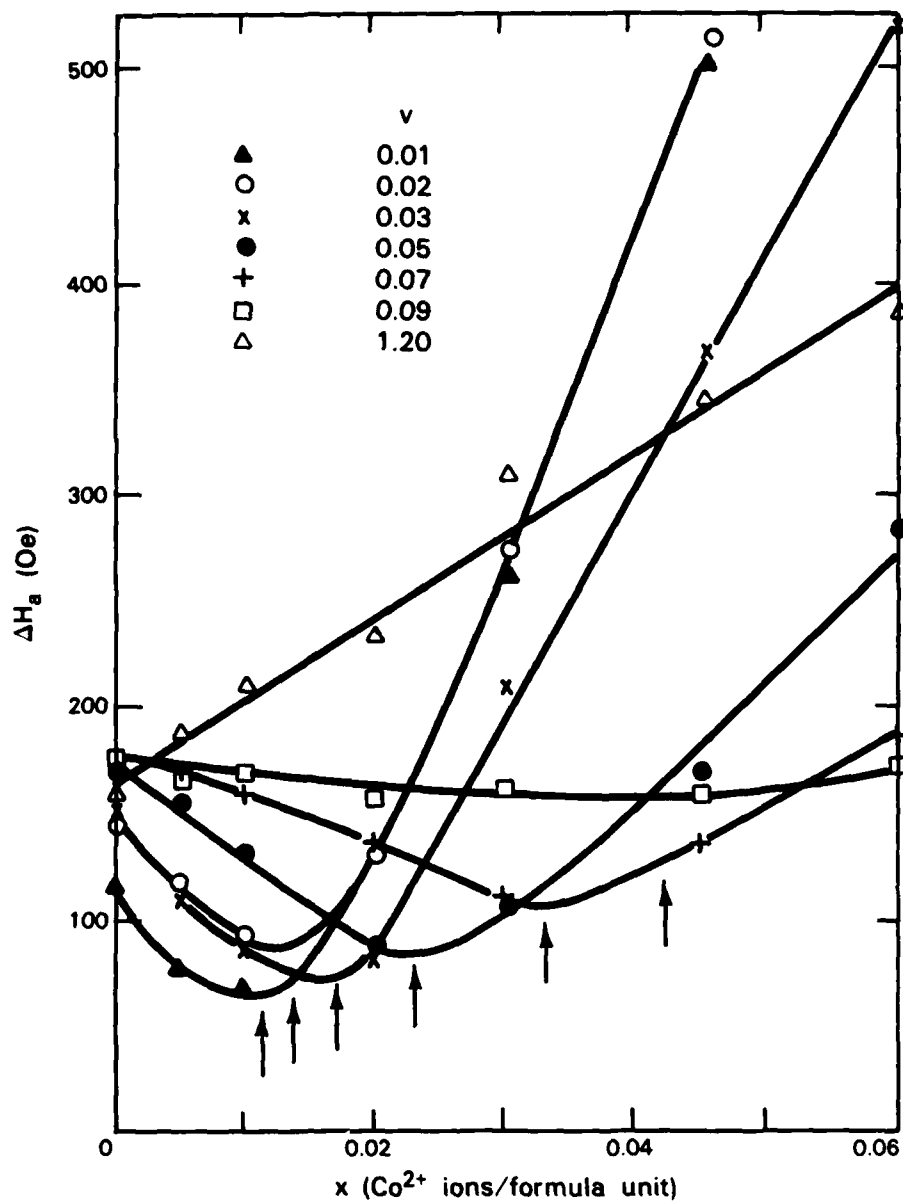


Figure 16. Effects of Co^{2+} on the anisotropy linewidth ΔH_a in $\{\text{Y}_{1.5-2v}\text{Gd}_{1.5}\text{Ca}_{2v}\}[\text{Fe}_{2-x}\text{Co}_x](\text{Fe}_{3-x-v}\text{Si}_x\text{V}_v)\text{O}_{12}$ vanadate garnets, after Llabres et al. [6].

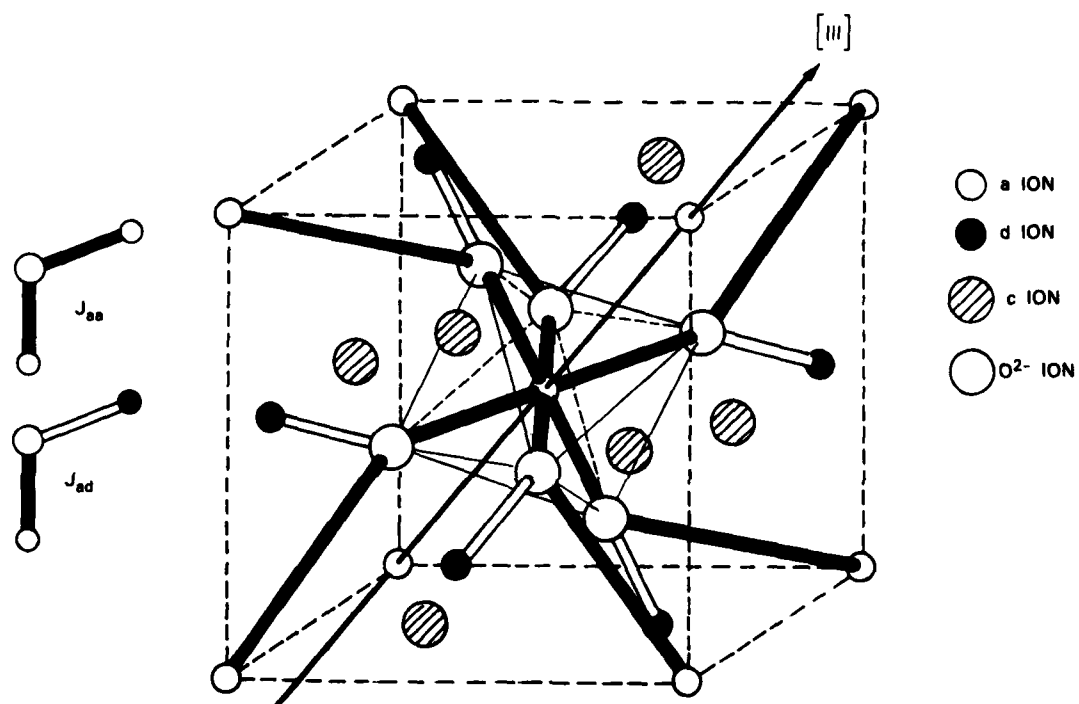


Figure 17. Partial unit cell of garnet lattice.

142106-P

existing crystal fields. In at least one instance, however, cation clustering of the type described for LiTi ferrite probably occurs. In the calcium vanadate garnet system, V^{5+} ions are used in combination with Ca^{2+} to reduce the magnetization of the dominant d sublattice. Here the V^{5+} ions occupy d sites and the Ca^{2+} ions replace Y^{3+} or other rare-earth ions in the c sublattice. Therefore, the crystal field component from a complete complement of $Ca^{2+}-V^{5+}$ ions in the nearest neighbor c and d sites surrounding a Co^{2+} site will be negative (opposite in sign to the LiTi ferrite case) and reinforcing the small trigonal field from the O^{2-} octahedron that accounts for at least part of the normal garnet anisotropy [36].

With an enhanced negative trigonal crystal field caused by this clustering, the energy levels of the lowest three orbital states of Fig. 13 would be inverted and a singlet ground state would result. Under these conditions, a crystal field stabilization of $2\Delta/3$ may be expected without a major change in the Co^{2+} anisotropy or relaxation properties as long as the splitting is small compared with the spin-orbit coupling energy. As a consequence, preferential V^{5+} occupation of the adjacent d sites would be energetically favorable and the Co^{2+} ion would become decoupled from the d sublattice. Although there was no dilution of the a sublattice in the compositions of Fig. 16, the isolation of cobalt from the iron could have been accomplished by balancing

the contributions of the a and d sublattices to the exchange field, i.e. $Q \rightarrow 0$ in Eq. (A-5), leading to vanishing values of k_C .

It should be noted that the concentration of Co^{2+} required for anisotropy compensation in Fig. 16 begins to increase for V^{5+} concentrations as low as 0.02 per formula unit and that the decoupling of cobalt is effectively complete by $v = 0.09$. For isolation effects to appear at such small concentrations of vanadium, the clustering of Ca^{2+} - V^{5+} originally suggested in earlier work by the author [22] must take place around the cobalt ions through crystal field stabilization in addition to exchange energy and cation charge balance mechanisms. Further evidence of this phenomenon may be inferred from Krishnan and Cagan's failure to find Co^{2+} positive anisotropy effects in vanadate garnet single crystals, while observing magnetostriction changes from Co^{2+} of the type predicted by the local site distortion model [37]. Since Jahn-Teller distortions in octahedral sites would be independent of magnetic exchange couplings, the magnetostriction effects should be present regardless of the distribution of surrounding cations.

Based on the data available for the garnet lattice, the Co^{2+} ion's reduced tendency for magnetocrystalline anisotropy cancellation in the presence of Ca^{2+} and V^{5+} dilutants, while retaining its rapid spin-lattice relaxation and local site magnetostriction properties, strongly suggests that the exchange isolation effect

proposed for Co^{2+} in LiTi spinel ferrites also occurs in this garnet system.

APPENDIX A

DEPENDENCE OF ANISOTROPY ON Co^{2+} EXCHANGE COUPLING

In the spinel lattice, Co^{2+} in a B site is coupled to six neighboring A sites and six neighboring B sites through super-exchange interactions through O^{2-} ions. In general terms, the total energy E is the sum of three contributions as follows,

$$E = E_k + E_{\text{ex}} + E_h, \quad (\text{A-1})$$

where E_k is the magnetocrystalline anisotropy energy, E_{ex} is the exchange energy, and E_h is the energy of interaction with an internal magnetic field \hat{H} . These individual terms may be expressed as:

$$\begin{aligned} E_k &= -\sum_i \frac{1}{2} k_i (\cos^2 \theta_i - \frac{1}{3}), \\ E_{\text{ex}} &= -2 \sum_j J_{ij} \hat{S}_i \cdot \hat{S}_j, \\ E_h &= -\sum_i \hat{H} \cdot \hat{S}_i, \end{aligned} \quad (\text{A-2})$$

where k_i is a single-ion anisotropy energy, \hat{S}_i and \hat{S}_j are spin vectors of individual ions i and j , and θ_i is the angle between \hat{S}_i and the [001] cubic axis. J_{ij} is the exchange constant between the i and j spins.

To examine the relation between these individual terms for a single cobalt ion, only the n_A and n_B cations coupled directly to

the Co^{2+} ion need to be considered. For the general case of \vec{H} at an angle θ to the [001] axis, Eq. (A-2) may be rewritten:

$$E_k = -\frac{1}{2} k_C (\cos^2 \theta_C - \frac{1}{3}) - \frac{1}{2} n_A k_A (\cos^2 \theta_A - \frac{1}{3}) - \frac{1}{2} n_B k_B (\cos^2 \theta_B - \frac{1}{3}),$$

$$E_{\text{ex}} = -2n_A J_{AC} S_A S_C \cos(\theta_A - \theta_C) - 2n_B J_{BC} S_B S_C \cos(\theta_B - \theta_C) \quad (\text{A-3})$$

$$- (n'_A + n'_B) J_{AB} S_A S_B \cos(\theta_A - \theta_B),$$

$$E_h = -H [S_C \cos(\theta - \theta_C) + n_A S_A \cos(\theta - \theta_A) + n_B S_B \cos(\theta - \theta_B)].$$

where n'_A and n'_B refer to the numbers of n_A and n_B that exchange couple to each other. A pictorial representation of this system is shown in the three-ion model of Fig. 9, where only one each of the six A and six B site neighbors are included.

With Fe^{3+} ions occupying most of the cation sites, in a magnetically saturated state the strong exchange fields will determine that $\theta_B = \theta$, $\theta_A = \theta - \pi$, where the B sublattice dominates. In this situation, Eq. (A-1) becomes

$$E = -\frac{1}{2} k_C (\cos^2 \theta_C - \frac{1}{3}) - \frac{1}{2} (n_A k_A + n_B k_B) (\cos^2 \theta - \frac{1}{3})$$

$$+ Q \cos(\theta - \theta_C) + (n'_A + n'_B) J_{AB} S_A S_B + H (n_A S_A - n_B S_B), \quad (\text{A-4})$$

where

$$Q = 2S_C (n_A J_{AC} S_A - n_B J_{BC} S_B - H). \quad (\text{A-5})$$

For any fixed value of θ , θ_C can be determined by minimizing the total system energy, so that

$$\frac{\partial E}{\partial \theta_C} = \frac{1}{2} k_C \sin 2\theta_C - Q \sin(\theta - \theta_C) = 0. \quad (\text{A-6})$$

Eq. (A-6) may then be solved by iteration in the form

$$\sin\theta_C = \frac{1}{\sqrt{3}} \frac{Q}{k_C} (\sqrt{2} - \tan\theta_C), \quad (\text{A-7})$$

and the variation of θ_C with Q is plotted in Fig. 18. Thus, the energy E may now be calculated from Eq. (A-4) for any value of Q/k_C and the first-order anisotropy energy may be found from E as \vec{H} is rotated between an easy and a hard magnetic direction. An easy axis for spinels (and garnets) would normally be the [111] direction, at $\theta = 54.74^\circ$, and a hard axis, the [001] direction at $\theta = 0$. In this manner, the effective contribution k_C' of a Co^{2+} ion to the total anisotropy constant of the Fe^{3+} sublattices in spinels was calculated as a fraction of its actual value k_C and plotted as a function Q/k_C in Fig. 10.

Since k_C' becomes small only when $Q/k_C < 1$, it is important to note that this condition can arise whenever $n_A J_{AC} S_A = n_B J_{BC} S_B$ (assuming that H is negligibly small) in Eq. (A-5). For Fe^{3+} ions, S_A and $S_B = 5/2$, n_A and $n_B \approx 6$ in most undiluted situations, but $|J_{AC}| > |J_{BC}|$ according to the molecular-field coefficients reported earlier [20]. This suggests that $n_A, n_B \rightarrow 0$ for complete isolation to occur. The sign of J_{ij} is always negative because superexchange coupling is antiferromagnetic, so that the sign of Q would always be negative regardless of which sublattice dominates. If $|n_A J_{AC}| < |n_B J_{BC}|$, the spin directions would reverse to maintain a minimum energy condition.

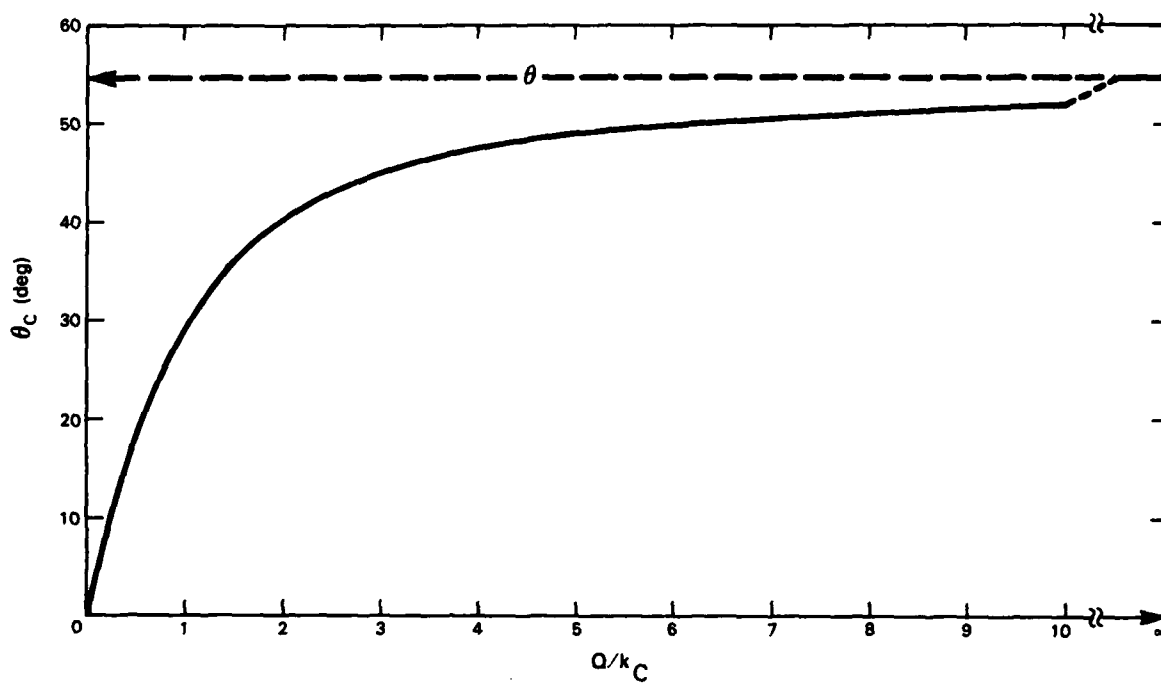


Figure 18. Co^{2+} spin polar angle θ_C as a function of θ/k_C .

142107-N

APPENDIX B

OXYGEN PARAMETER CALCULATIONS

For spinels, there are two crystallographic dimensions normally used to characterize the unit cell. The first is the lattice parameter or cubic unit cell dimension a_o , and the second is the oxygen parameter u , which is defined by the distance from a tetradhedral O^{2-} ion to the farther plane containing its nearest neighbor tetrahedral cations [38]. This distance is ua_o , where u would be $3/8$ for a lattice without distortion. In terms of the radii of the ions occupying the A and B sites, the following relations for a_o and u were obtained from the geometry of the spinel lattice [39]:

$$a_o = 3(R_B + R_{OB}) + \frac{2}{\sqrt{3}} (R_A + R_{OA}) , \quad (B-1)$$

$$u = \frac{(R_A - R_B) + (R_{OA} - R_{OB}) + (\sqrt{3}/4 + 5/8)a_o}{(\sqrt{3} + 1)a_o} , \quad (B-2)$$

where R_A and R_B are the radii of the A and B cations, and R_{OA} and R_{OB} are the radii of O^{2-} in tetradedral and octahedral coordinations, respectively.

To begin the calculations, the measured values of $a_o = 8.337$ Å [40] and $u = 0.382$ [41] for $Li_{0.5}Fe_{2.5}O_4$ were chosen, together with the O^{2-} radii $R_{OA} = 1.38$ Å and $R_{OB} = 1.40$ Å derived by Shannon and Prewitt (S-P) from a wide collection of

published data [42]. From Eq. (B-2), $R_A - R_B = -0.140$ and is in reasonable agreement with the value of -0.11 determined by Zachariaisen [43]. By appropriate substitution into Eq. (B-1), the individual radius values corresponding to these two sites are found to be $R_A = 0.511 \text{ \AA}$ and $R_B = 0.651 \text{ \AA}$, in very favorable agreement with the SP Fe^{3+} radii of 0.49 and 0.645 \AA , respectively. Since 25 percent of the B-site cations are Li^{1+} in this compound, it appears that the Li^{1+} radii are approximately the same as those of Fe^{3+} in this particular lattice and should be treated as such for all practical purposes.

For the case of a Co^{2+} ion in a B site surrounded by Li^{1+} in neighboring A sites, we should expect no significant change in R_A , but an increase in R_B from 0.651 \AA to 0.745 \AA (S-P Co^{2+} value). Applying Eqs. (B-1) and (B-2), we find that local to the Co^{2+} site, a_o increases from 8.337 to 8.519 \AA and u decreases from 0.382 to 0.376 , a value closely approaching the 0.375 of the ideal case. Thus, we may conclude that the octahedral distortion is reduced greatly and the negative trigonal field component likely present at B sites in pure $\text{Li}_{0.5}\text{Fe}_{2.5}\text{O}_4$ may be almost neutralized locally by the substitution of the larger Co^{2+} ions.

APPENDIX C

d-ORBITAL WAVE FUNCTIONS IN AXIAL CRYSTAL FIELDS

In crystal electric fields, the orbital energy level structure of transition-metal ions can be determined by analytical methods usually involving group theory or operator equivalent perturbation techniques. In general, group theory will enable one to establish the energy degeneracies and eigenfunctions of the orbital levels, but perturbation calculations are necessary to fix the order of the level structure. One useful tool has proven to be graphical representations of the orbital eigenfunctions inside the ligand coordinations, where the proximities of the orbital lobes to the ligand charges provide insight into the relative energies of the states.

For the case of a tetragonally distorted octahedron of ligands, with the axis of quantization (z-axis) along a four-fold symmetry direction, the d-electron orbital eigenfunctions (with radial part and common factors omitted) may be expressed as [44]

$$t_{2g}^x = \sqrt{3} yz$$

$$t_{2g}^y = \sqrt{3} xz$$

$$t_{2g}^z = \sqrt{3} xy \quad (C-1)$$

$$e_g^z = \frac{1}{2} (2z^2 - x^2 - y^2)$$

$$e_g^{xy} = \frac{\sqrt{3}}{2} (x^2 - y^2) .$$

By means of computer graphics techniques, these functions were plotted in three dimensions in Fig. 19 using spherical coordinates. A typical procedure was to hold the polar angle θ (referred to the z axis) constant and trace a section by varying the azimuthal angle ϕ (referred to the x axis) in 5-degree increments. A series of these sections at equal intervals of θ then mapped out the orbital lobes.

From the directions of the electron orbital lobes in relation to the locations of the O^{2-} ligands along the x,y and z axes, it can be seen how the higher energy doublet E_g and lower energy triplet T_{2g} occur (see Fig. 13a). It is also readily discernible that a distortion along the z axis would lift the degeneracy of E_g and also separate the T_{2g} triplet by splitting off t_{2g}^z from t_{2g}^x and t_{2g}^y .

Although the above example has been used in standard texts [45], it does not represent a situation that appears often in practical systems. The more common occurrence is where the distortion is trigonal (along a $\langle 111 \rangle$ body diagonal axis), as is the case for spinels, garnets and alum salts [46,47]. For the three-fold symmetry of a trigonal perturbation, the orbitals of Eq. (C-1) are no longer eigenfunctions. A more suitable set with the same z axis of quantization is similar to the set used by Pryce and Runciman [48]. These linear combinations were formed within

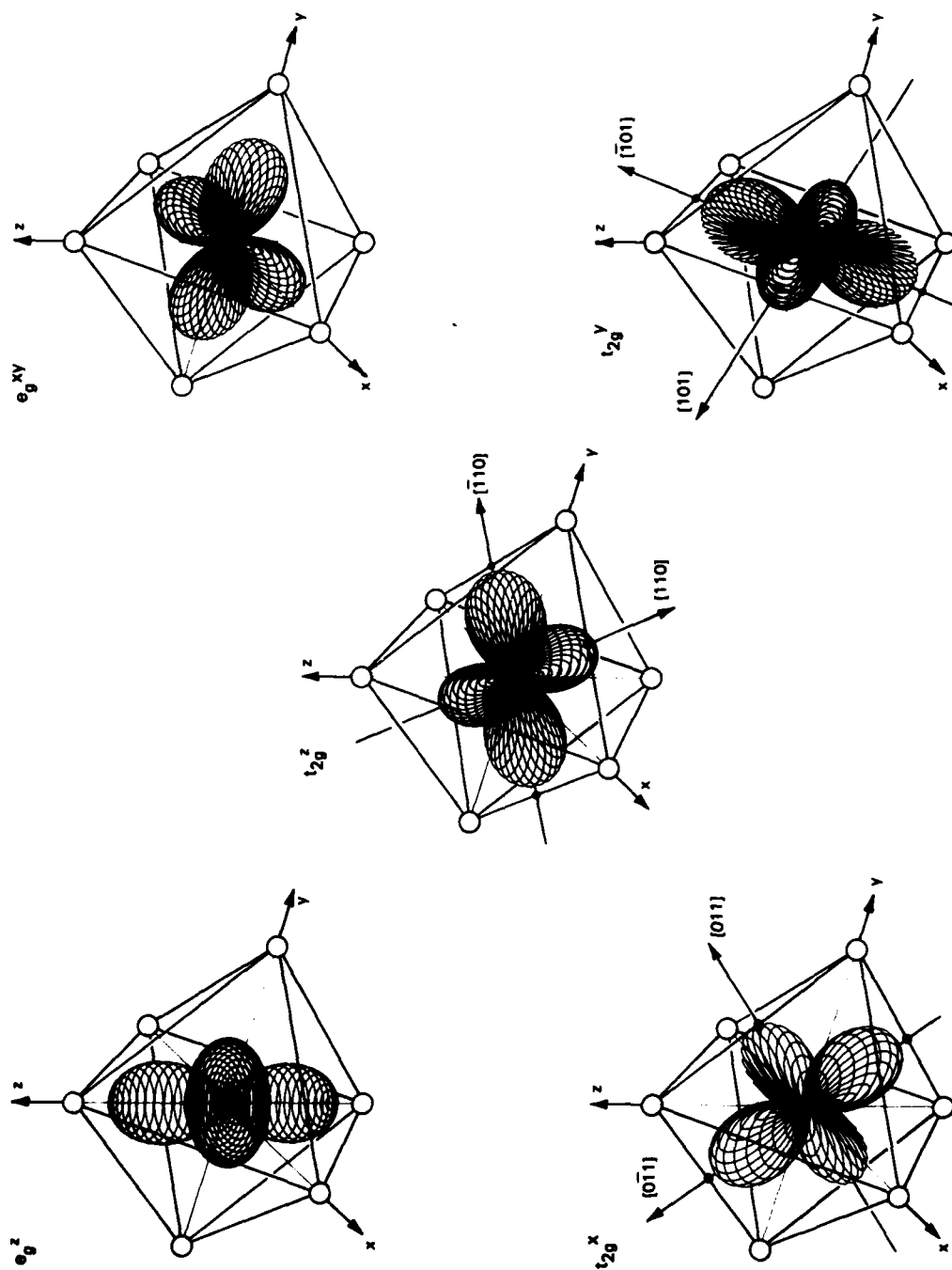


Figure 19. d-electron orbital wave functions for tetragonal crystal field, with [001] axis of symmetry.

the T_{2g} and E_g groups of the tetragonal set by rotations of the functions in Eq. (C-1) according to

$$\begin{pmatrix} t_{2g}^0 \\ t_{2g}^+ \\ t_{2g}^- \end{pmatrix} = \begin{pmatrix} 1/\sqrt{3} & 1/\sqrt{3} & 1/\sqrt{3} \\ 1/\sqrt{2} & -1/\sqrt{2} & 0 \\ 1/\sqrt{6} & 1/\sqrt{6} & -\sqrt{2/3} \end{pmatrix} \begin{pmatrix} t_{2g}^x \\ t_{2g}^y \\ t_{2g}^z \end{pmatrix}$$

$$\begin{pmatrix} e_g^+ \\ e_g^- \end{pmatrix} = \begin{pmatrix} 1/\sqrt{2} & 1/\sqrt{2} \\ -1/\sqrt{2} & 1/\sqrt{2} \end{pmatrix} \begin{pmatrix} e_g^z \\ e_g^{xy} \end{pmatrix}, \quad (C-2)$$

resulting in

$$\begin{aligned} t_{2g}^0 &= xy + yz + xz \\ t_{2g}^+ &= \frac{\sqrt{3}}{\sqrt{2}} (yz - xz) \\ t_{2g}^- &= \frac{1}{\sqrt{2}} (2xy - yz - xz) \\ e_g^+ &= \frac{1}{\sqrt{2}} (Ax^2 + By^2 + z^2) \\ e_g^- &= -\frac{1}{\sqrt{2}} (Bx^2 + Ay^2 + z^2), \end{aligned} \quad (C-3)$$

where $A = \frac{1}{2} (\sqrt{3} - 1)$ and $B = -\frac{1}{2} (\sqrt{3} + 1)$.

The graphical displays of these wave functions for a trigonal distortion along the $[\bar{1}11]$ direction (i.e. $x \rightarrow -x$ in Eq. (C-3)) are given in Fig. 20, where the upper doublet E_g remains degenerate, while the T_{2g} set splits into a t_{2g}^0 singlet and a t_{2g}^+ , t_{2g}^- doublet. The lobes of e_g^+ and e_g^- are directed towards the ligands and are identical except for the reversal of x and y axes. With respect to the $[\bar{1}11]$ distortion axis, the orbitals are equivalent. The t_{2g}^0 orbital, however, is similar in shape to eg_z , but directed along the trigonal axis. The equal lobes of t_{2g}^+ are along directions with $\theta = \pm 45^\circ$ and $\phi = 45^\circ$. The main t_{2g}^- lobe points along a direction with $\theta = 62.6^\circ$ and $\phi = -45^\circ$, and the smaller one along the $[110]$ axis in the x - y plane. Since the lobes of both of these orbital wave functions are directed away from the ligands and also away from the trigonal distortion axis, the degeneracy expected from group theory is at least suggested by these plots. In this manner, the t_{2g}^+ and t_{2g}^- orbitals would be of different energy than t_{2g}^0 for a $[\bar{1}11]$ distortion and remain degenerate.

In conclusion, it should be repeated that the wave functions of Eqs. (C-1) and (C-3) are equivalent sets of eigenfunctions in the cubic field. When a distortion is along the $[001]$ axis, the initial set is the correct one; when along the $[\bar{1}11]$ axis, it is the new set of Eq. (C-3) that should be used.

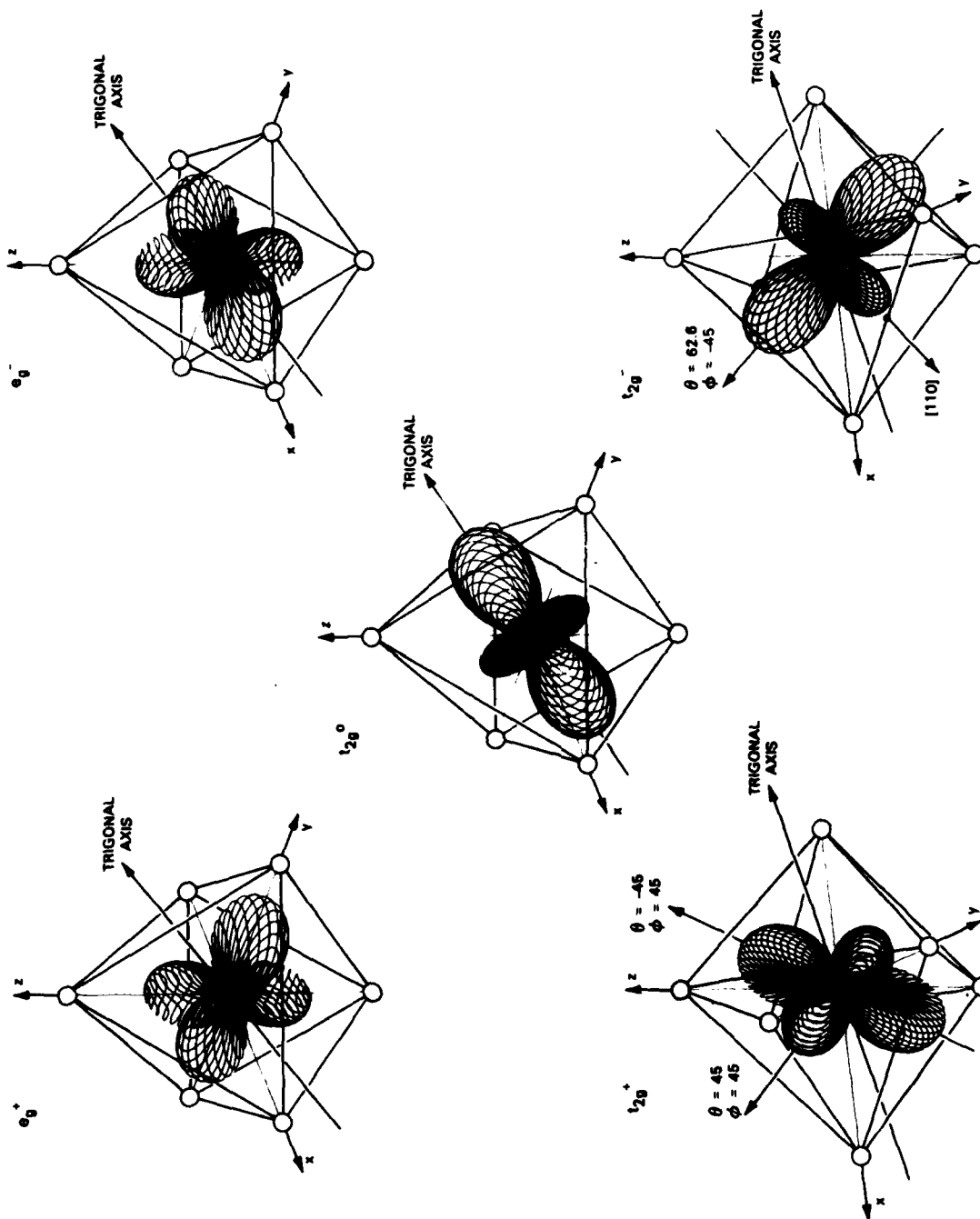


Figure 20. d-electron orbital wave functions for trigonal crystal field, with $[\bar{1}11]$ axis of symmetry.

142102-R

APPENDIX D

EFFECTS OF Zn^{2+} ON MAGNETIZATION AND ANISOTROPY FIELDS OF LiTi FERRITE

For the ferrite system described by the general formula $\text{Li}_{t/2-z/2}\text{Zn}_z\text{Fe}_{1-t/2-z/2}[\text{Li}_{0.5}\text{Ti}_t\text{Fe}_{1.5-t}]\text{O}_4$, the substitution of Zn^{2+} affects the concentrations of both Li^{1+} and Fe^{3+} in the A sublattice. If we make the approximation that the magnetization and anisotropy are determined by the addition of single-ion contributions at any particular temperature, and are unaffected by canting effects caused by concentration-dependent molecular field coefficients [20], the following model may be constructed.

The general equations for magnetization M_s and anisotropy K_1 may be written as:

$$\begin{aligned} M_s &= M_B(1 - 1/4 - t/2) - M_A(1 - t/2 - z/2) \\ K_1 &= K_B(1 - 1/4 - t/2) - K_A(1 - t/2 - z/2), \end{aligned} \quad (\text{D-1})$$

where the A and B subscripts refer to the respective sublattices. Since Eq. (D-1) is based on the model of a total Fe^{3+} occupation of both sublattices, we may also assume that $M_B = 2M_A$. In addition, since most of the anisotropy of the Fe^{3+} originates in the B sublattice [49], we may assume that $K_B \gg K_A$ and Eq. (D-1) may be reduced to

$$M_S = (1/2) M_A (1 - t + z)$$

$$K_1 \approx (1/2) K_B (3/2 - t) . \quad (D-2)$$

Thus, it may be concluded that the immediate effect of a Zn^{2+} substitution is an increase in the magnetization. The anisotropy field H_A is then reduced according to

$$H_A = \frac{2K_1}{M_S} \approx \frac{2K_B}{M_A} \left(\frac{3/2 - t}{1 - t + z} \right) . \quad (D-3)$$

In situations where the magnetization remains unchanged by a compensating increase t' in titanium concentration, Eq. (D-2) becomes

$$M_S = (1/2) M_A (1 - t - t' + z)$$

$$K_1 \approx (1/2) K_B (3/2 - t - t') . \quad (D-4)$$

Since M_S must remain unchanged, $t' = z$ and Eq. (D-4) may be simplified to

$$M_S = (1/2) M_A (1 - t)$$

$$K_1 \approx (1/2) K_B (3/2 - t - z) , \quad (D-5)$$

and the anisotropy field for this case would be

$$H_A \approx \frac{2K_B}{M_A} \left(\frac{3/2 - t - z}{1 - t} \right) . \quad (D-6)$$

In comparing Eqs. (D-3) and (D-6), it is interesting to observe that the anisotropy field reduction is accomplished in the initial case by an increase in M_S , and in the case where M_S

is unchanged, by a decrease in K_1 . The implications of this result would depend on the relative importance K_1 and $2K_1/M_s$ for the intended properties of the material.

ACKNOWLEDGMENTS

The author is grateful to James F. Fitzgerald for assistance in the experimental part of this work and to Barbara J. Palm for writing the computer program to plot orbital wave functions. Appreciation is also expressed to Roger W. Sudbury for discussions helpful in designing the experiments, to Russell G. West of Trans-Tech Inc. for furnishing measurement data, and to John Mather, Dr. H. Jerrold Van Hook and J. Dawson Milne of the Raytheon Company for carrying out the magnetic loss measurements.

REFERENCES

1. R.M. Bozorth, E.F. Tilden, and A.J. Williams, Phys. Rev. 99, 1788 (1955).
2. L.R. Bickford, J.M. Brownlow, and R.F. Penoyer, Proc. Inst. Elec. Engrs. London 104B, Suppl. No. 5, 238 (1957).
3. P.D. Baba, G.M. Argentina, W.E. Courtney, G.F. Dionne, and D.H. Temme, IEEE Trans. Mag. MAG-8, 83 (1972).
4. C.J. Brower and C.E. Patton, J. Appl. Phys. 53, 2104 (1982).
5. G.F. Dionne and J.B. Goodenough, Mat. Res. Bull. 7, 749 (1972).
6. J. Llabres, J. Nicolas, and R. Sproussi, Appl. Phys. 12, 87 (1977).
7. R. Krishnan, Phys. Stat. Solid. (B) 35, K63 (1969).
8. R. Krishnan and V. Cagan, Ferrites, Proc. Intl. Conf. (Japan, 1970), p. 57.
9. J.J. Green and E. Schloemann, IEEE Trans. Microwave Theory Tech. MTT-8, 100 (1960).
10. C.J. Jefferson and R.G. West, J. Appl. Phys. 32, 390S (1961).
11. J.J. Green and H.J. Van Hook, IEEE Trans. Microwave Theory Tech. MTT-25, 155 (1977).
12. C.E. Patton, D.L. Blankenbeckler, C.J. Brower, B.B. Dalton, and A.M. Lucero, IEEE Trans. Mag. MAG-17, 2976 (1981).
13. H.J. Van Hook and G.F. Dionne, Proc. 20th Conf. Mag. & Magnetic Materials (1974), AIP Conf. Proc. No. 24, (1975), p. 487.
14. M.A. Stelmashenko and N.V. Seleznev, Sov. Phys. J. 2, 7 (1966).
15. S.K. Banerjee, P.D. Baba, B.J. Evans, and S.S. Hafner, J. de Physique, Coll. C1, 145 (1971).

16. J.J. Green and F. Sandy, IEEE Trans. Microwave Theory Tech. MTT-22, 645 (1974).
17. J.A. Weiss and F. Betts, J. Appl. Phys. 38, 1397 (1967).
18. J.C. Slonczewski, Phys. Rev. 110, 1341 (1958).
19. J.B. Goodenough, Magnetism and the Chemical Bond, (John Wiley, 1963), pp. 165-185.
20. G.F. Dionne, J. Appl. Phys. 45, 3621 (1974); Technical Report TR-502, Lincoln Laboratory, M.I.T. (10 May 1974), AD-782421/2.
21. G.F. Dionne, J. Appl. Phys. 40, 1839 (1969).
22. G.F. Dionne, Mat. Res. Bull. 7, 1393 (1972).
23. E. Schloemann and T. Kohane, J. Appl. Phys. 38, 1118 (1967); Technical Memorandum T-688, Research Division, Raytheon Company (1966).
24. E.J.W. Verwey and E.L. Heilmann, J. Chem. Phys. 15, 174 (1947).
25. F. de Boer, J.H. Van Santen, and E.J.W. Verwey, J. Chem. Phys. 18, 1032 (1950).
26. L.E. Orgel, An Introduction to Transition-Metal Chemistry, (John Wiley, 1966), p. 30-35.
27. G.F. Dionne, J. Appl. Phys. 40, 3061 (1969).
28. J.H. Van Vleck, J. Appl. Phys. 35, 882 (1964).
29. P.G. de Gennes, C. Kittel, and A.M. Portis, Phys. Rev. 116, 323 (1959).
30. G.F. Dionne, J. Appl. Phys. 40, 431 (1969).
31. P. Beuzelin, P. Feldmann, and W. Simonet, IEEE Trans. Mag. MAG-17, 3135 (1981).
32. R.D. Mattuck and M.W.P. Strandberg, Phys. Rev. 119, 1204 (1960).
33. K.J. Standley and R.A. Vaughan, Electron Spin Relaxation Phenomena in Solids, (Plenum Press, 1969), Chapter 3.

34. E. Schloemann, J.J. Green, and V. Milano, J. Appl. Phys. 31, 386S (1960).
35. G.F. Dionne and R.G. West, Proc. 18th Conf. Mag. & Mag. Materials, AIP Conf. Proc. No. 10 (1973), p. 169.
36. W.P. Wolf, Phys. Rev. 108, 1152 (1957).
37. G.F. Dionne, J. Appl. Phys. 50, 4263 (1979); Technical Report TR-532, Lincoln Laboratory, M.I.T. (29 November 1978), AD-AO66250/2.
38. J. Smit and H.P.J. Wijn, Ferrites, (John Wiley, 1959), p. 138.
39. Ibid, p. 140.
40. J. Schieber, J. Inorg. Nucl. Chem. 26, 1363 (1964).
41. P.B. Braun, Nature 170, 1123 (1952).
42. R.D. Shannon and C.T. Prewitt, Acta Cryst. B25, 925 (1969).
43. C. Kittel, Introduction to Solid State Physics, (John Wiley, 1966) p. 105.
44. C.J. Ballhausen, Introduction to Ligand Field Theory, (McGraw-Hill Book Co. 1962), p. 64.
45. S. Chikazumi, Physics of Magnetism, (John Wiley, 1964), p. 154.
46. J.H. Van Vleck, Disc. Faraday Soc. 26, 96 (1958).
47. G.F. Dionne and J.A. MacKinnon, Phys. Rev. 172, 325 (1968).
48. M.H.L. Pryce and W.A. Runciman, Disc. Faraday Soc. 26, 34 (1958).
49. K. Yosida and M. Tachiki, Prog. Theoret. Phys. 17, 331 (1957).

UNCLASSIFIED

SECURITY CLASSIFICATION OF THIS PAGE (When Data Entered)

REPORT DOCUMENTATION PAGE		READ INSTRUCTIONS BEFORE COMPLETING FORM
1. REPORT NUMBER ESD-TR-84-034	2. GOVT ACCESSION NO. <i>A46550</i>	3. RECIPIENT'S CATALOG NUMBER
4. TITLE (and Subtitle) Anisotropy and Relaxation Effects of Co^{2+} Ions in LiTi Ferrite		5. TYPE OF REPORT & PERIOD COVERED Technical Report
		6. PERFORMING ORG. REPORT NUMBER Technical Report 688
7. AUTHOR(s) Gerald F. Dionne		8. CONTRACT OR GRANT NUMBER(s) F19628-80-C-0002
9. PERFORMING ORGANIZATION NAME AND ADDRESS Lincoln Laboratory, M.I.T. P.O. Box 73 Lexington, MA 02173-0073		10. PROGRAM ELEMENT, PROJECT, TASK AREA & WORK UNIT NUMBERS Program Element No. 63308A
11. CONTROLLING OFFICE NAME AND ADDRESS Ballistic Missile Defense Sentry Project Office Department of the Army P.O. Box 15280 Arlington, VA 22215		12. REPORT DATE 15 August 1984
		13. NUMBER OF PAGES 74
14. MONITORING AGENCY NAME & ADDRESS (if different from Controlling Office) Electronic Systems Division Hanscom AFB, MA 01731		15. SECURITY CLASS. (of this report) Unclassified
		15a. DECLASSIFICATION DOWNGRADING SCHEDULE
16. DISTRIBUTION STATEMENT (of this Report) Approved for public release; distribution unlimited.		
17. DISTRIBUTION STATEMENT (of the abstract entered in Block 20, if different from Report)		
18. SUPPLEMENTARY NOTES None		
19. KEY WORDS (Continue on reverse side if necessary and identify by block number)		
<div style="display: flex; justify-content: space-between;"> <div> lithium-titanium ferrite high-power effects magnetic exchange isolation </div> <div> cobalt anisotropy and relaxation hysteresis loops cation clustering </div> </div>		
20. ABSTRACT (Continue on reverse side if necessary and identify by block number)		
<p>Microwave power absorption and hysteresis loops were studied on a series of ferrite materials prepared from a standard LiTi spinel host with Co^{2+} additions in amounts up to 0.05 ions per formula unit. The usual strong effects of Co^{2+} positive magnetic anisotropy were not found in either ferrimagnetic resonance linewidths or hysteresis loop parameters. As a consequence, it is concluded that peak power thresholds can be raised substantially by Co^{2+} additions with a modest penalty in magnetic loss, but without the catastrophic deterioration of the hysteresis loop observed previously in undiluted lithium ferrite.</p> <p>To account for the absence of anisotropy effects in the presence of strong relaxation effects, Co^{2+} is considered to act as a paramagnetic ion through decoupling from the exchange fields of the iron sublattices. This new theory of exchange isolation is based on selective clustering of dilutant ions that results from minimization of magnetic exchange, lattice electrostatic, and crystal field stabilization energies.</p>		

UNCLASSIFIED

SECURITY CLASSIFICATION OF THIS PAGE (When Data Entered)

END

FILMED

1-84

DTIC